ACS APPLIED MATERIALS & INTERFACES

Research Article

www.acsami.org

Fluorene-Based Sensitizers with a Phenothiazine Donor: Effect of Mode of Donor Tethering on the Performance of Dye-Sensitized Solar Cells

Abhishek Baheti,[†] K. R. Justin Thomas,*[,†] Chun-Ting Li,[#] Chuan-Pei Lee,[#] and Kuo-Chuan Ho[#]

[†]Organic Materials Laboratory, Department of Chemistry, Indian Institute of Technology Roorkee, Roorkee, Uttarakhand 247 667, India

[#]Department of Chemical Engineering, National Taiwan University, Taipei 10617, Taiwan

Supporting Information

ABSTRACT: Two types of fluorene-based organic dyes featuring T-shape/rod-shape molecular configuration with phenothiazine donor and cyanoacrylic acid acceptor have been synthesized and characterized as sensitizers for dye-sensitized solar cells. Phenothiazine is functionalized at either nitrogen (N10) or carbon (C3) to obtain T-shape and rod-like organic dyes, respectively. The effect of structural alternation on the optical, electrochemical, and the photovoltaic properties is investigated. The crystal structure determination of the dye containing phenyl linker revealed cofacial slip-stack columnar packing of the molecules. The trends in the optical properties of the dyes are interpreted using time-dependent density functional theory (TDDFT) computations. The rod-shaped dyes exhibited longer wavelength absorption and low oxidation potentials when compared to the corresponding T-shaped dyes attributable to the favorable electronic overlap between the phenothiazine unit and the rest of the molecule in the former dyes. However, the T-shaped dyes showed better photovoltaic properties due to the lowest unoccupied molecular orbital (LUMO) energy level favorable for electron injection into the conduction band of TiO_2 and appropriate orientation of the phenothiazine unit rendering effective surface blocking to suppress the recombination of electrons between the electrolyte I_3^- and TiO_2. The electrochemical impedance spectroscopy investigations provide further support for the variations in the electron injection and transfer kinetics due to the structural modifications.

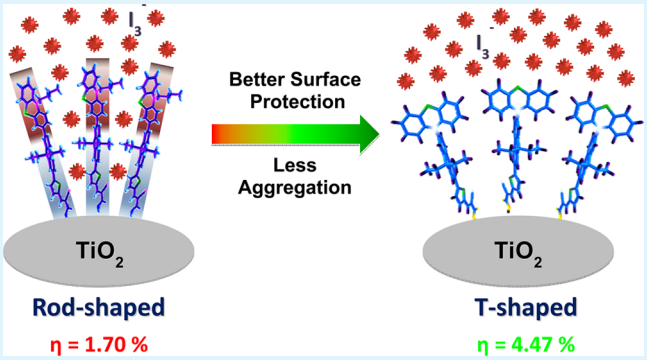

KEYWORDS: *phenothiazine, organic dyes, optical spectra, TDDFT computations, dye-sensitized solar cells, electrochemical impedance spectroscopy*

INTRODUCTION

Recently, dye sensitized solar cells (DSSCs)[1] have attracted much attention as an alternative to p−n junction solar cells due to their low cost, easy fabrication, fairly high power conversion efficiency (PCE), and availability of large classes of sensitizers. A lot of investigations have been performed on the components of DSSC, including dye sensitizer, redox electrolyte, and inorganic semiconductor metal oxides.[2] Among all these, sensitizers have been recognized as one of the important constituents that influences the efficiency of the DSSC. Until now, metal-containing dyes such as ruthenium-based polypyridyl complexes,[3] porphyrins,[4] and perovskites[5] have been demonstrated to yield high solar energy to power conversion. However, some disadvantages limited their potential for large scale applications such as scarcity of platinum group metals, relatively high cost of production, and environmental hazardousness associated with lead. Despite the low lab scale efficiency reports, metal-free organic sensitizers[6−8] are attractive due to the relatively low production cost and facile synthetic methodologies. Also, they have displayed superiority over the ruthenium-based dyes in molar extinction coefficients for longer wavelength intramolecular charge transfer (ICT) absorption which can be further fine-tuned by easy chemical modifications.

Most of the organic dyes are designed with a simple donor-π-acceptor (D-π-A)[6−8] molecular configuration which facilitates effective photoinduced intramolecular charge transfer across the molecule. With this successful approach, a number of organic dyes featuring various arylamine donors[9] containing different conjugating bridges and cyanoacrylic acid acceptors have been synthesized for application in dye-sensitized solar cells. Although arylamine-based organic dyes have exhibited competitive efficiency (∼10%)[9] comparable to metal complexes (∼12%),[3] they still suffer from some disadvantages. The main

Received: September 9, 2014
Accepted: December 31, 2014
Published: December 31, 2014

DOI: 10.1021/am506149q
ACS Appl. Mater. Interfaces 2015, 7, 2249−2262

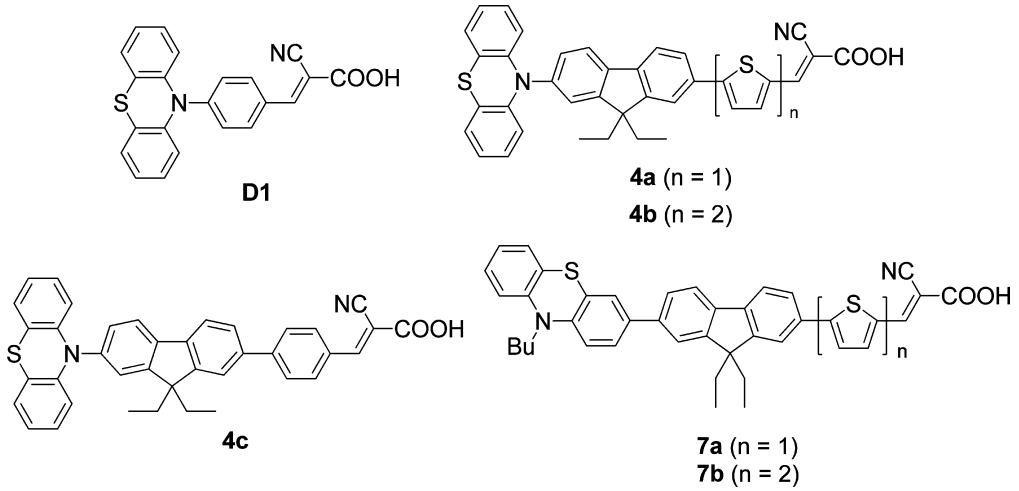

Figure 1. Structures of the dyes.

reasons for the efficiency deterioration of DSSC using organic dyes are their poor spectral response in the near-infrared region, probability of charge recombination at the semiconductor/electrolyte surface, and aggregation of sensitizers at the semiconductor surface.[2] It has been found that the extension of conjugation by incorporating electron donating or electron accepting moieties and integration of polyaromatic hydrocarbons in the conjugation pathway are useful approaches to bathochromically shift the absorption spectra,[10−12] while the introduction of longer alkyl chains or bulky substituents onto the π-bridge and slightly tilted spacer are found to be beneficial for charge collection and reducing charge recombination, despite the dyes displaying blue-shifted absorption.[13,14]

Recently, phenothiazine-derivatives have been increasingly used in light-emitting diodes (LEDs)[15] and photovoltaic devices[16] and as chemical sensors[17] owing to their excellent hole transporting ability, nonplanar geometry, and favorable thermal and electrochemical stability. Phenothiazine has also been used as a promising donor in the organic dyes used as sensitizers in DSSCs.[18−28] In most of them, the nitrogen atom (N10) is covalently attached with alkyl/aryl moiety and C3 carbon is used to link with the cyanoacrylic acid acceptor via heterocyclic units such as EDOT, thiophene, and furan.[19] Some reports explored the use of phenothiazine as a spacer via C3 and C7 carbons.[20] Hart et al.[21] synthesized two types of phenothiazine-based dyes, one having substitution on the C3 and another through the N-substitution (**D1**), and studied the effect of anchor substitution on the performance of DSSCs. They found that the oxidation potential for the N-substituted dye (**D1**) is lower than that of the C3 substituted dye and the lowest unoccupied molecular orbital (LUMO) energy is favorably positioned for the **D1**. This implies that the N-substituted dye possess more thermodynamic driving force for the charge injection into the conduction band (CB) of TiO_2. However, **D1** exhibited poor performance in DSSC attributable to its weak spectral response in the longer wavelength region. In another work, Hua et al.[22] synthesized two types of phenothiazine-based organic dyes in which donor aryl groups were appended at different positions, i.e., at C7 (type 1) and N10 (type 2). They found that donor aryl group at C7 position extends the conjugation of the chromophore while the donor aryl group at N10 significantly increases the steric hindrance of the dye. Consequently, type 1 dyes exhibit better light harvesting and higher PCE. Hua et al.[23] synthesized a series of phenothiazine-based organic dyes featuring (4-hexyloxy) phenyl donor moiety at the C7 position and the alkyl substituents with different chain length at the N10 position. When applied to DSSC, they found that the alkyl substituents provide shielding of the TiO_2 surface from the electrolyte and reduce dark current. Moreover, the length of alkyl chains significantly affected the PCE. Further, to study the effect of different electron donating groups on the performance of phenothiazine-based dyes, they introduced different thiophene derivatives at the C7 position as the donor and hexyl chain at the N10 position of phenothiazine.[24] They observed that the selection of different thiophene analogues affect the light absorption, alter the energy levels, influence the dye aggregation, and charge recombination properties.

In continuation of our interest in fluorene-containing dyes[29−34] and the benefit of fluorene-oligothiophene segment in improving the light harvesting properties and photocurrent density, we set out to explore phenothiazine end-capped dyes containing fluorene in the conjugation pathway. Also, the presence of fluorene in π-linker modulates the energy level and retards dye aggregation. These properties facilitate the regeneration of the dyes by the electrolyte and help to suppress the back reaction of the injected electrons with the oxidized dye. Herein, we have synthesized two types of novel fluorene-based D-π-A sensitizers featuring phenothiazine donor and cyanoacrylic acid as acceptor/anchoring group to investigate the positioning effect of a donor group in DSSC. In type 1 dyes (**4a**−**4c**), fluorene is attached to the phenothiazine donor via nitrogen atom resulting in T-shaped molecules while in the second type fluorene is linked to phenothiazine via C3 carbon producing rod-shaped dyes (**7a** and **7b**) (Figure 1). As the mode of attachment of phenothiazine will affect the effective conjugation length of the molecules, the electronic properties may be different in both types of dyes. We found that the T-shaped dyes exhibit better photovoltaic performance when compared to the rod-shaped dyes.

EXPERIMENTAL SECTION

General Methods. All reactions and manipulations were carried out under N_2 with the use of standard inert atmosphere and Schlenk techniques. Solvents were dried by standard procedures. All column chromatography purifications were performed with the use of 100−200 mesh silica gel as the stationary phase unless otherwise specified in a column of 30 cm length and 2.0 cm diameter. The ^1H and ^{13}C NMR

DOI: 10.1021/am506149q
ACS Appl. Mater. Interfaces 2015, 7, 2249−2262

spectra were measured by using a 500 MHz spectrometer. Mass spectra were recorded in positive-ion mode on an electrospray ionization (ESI) time of flight (TOF) high-resolution mass spectrometer. Electronic absorption spectra were obtained on a UV−visible spectrophotometer using freshly prepared solutions. Cyclic voltammetric experiments were carried out at room temperature with a conventional three-electrode configuration consisting of a glassy carbon working electrode, a platinum wire auxiliary electrode, and a nonaqueous $Ag/AgNO_3$ reference electrode. The $E_{1/2}$ values were determined as $1/2(E_p^a + E_p^c)$, where E_p^a and E_p^c are the anodic and cathodic peak potentials, respectively. The potentials are quoted against the ferrocene internal standard. The solvent in all experiments was dichloromethane, and the supporting electrolyte was 0.1 M tetrabutylammonium perchlorate.

10-(7-Bromo-9,9-diethyl-9H-fluoren-2-yl)-10H-phenothiazine, ***2***. A reaction flask was charged with 2,7-dibromo-9,9-diethyl-9*H*-fluorene (3.04 g, 8.0 mmol), 10*H*-phenothiazine (0.79 g, 4.0 mmol), sodium *tert*-butoxide (0.76 g, 7.83 mmol), $Pd(dba)_2$ (dba = (1*E*,4*E*)-1,5-diphenylpenta-1,4-dien-3-one; 46 mg, 0.08 mmol), 1,2-bis-(diphenylphosphino)ferrocene, (dppf; 44 mg, 0.08 mmol), and toluene (10 mL) under nitrogen atmosphere. The mixture was heated at 80 °C for 36 h. After the completion of the reaction, the volatiles were removed by rotary evaporation. The resulting residue was triturated with water and extracted with dichloromethane. The combined organic layer was dried over anhydrous sodium sulfate and evaporated in vacuum to produce a crude product. It was adsorbed on neutral alumina and purified by column chromatography by using a hexanes/dichloromethane (1:4) mixture as eluant. White solid; yield 1.32 g (66%). mp 168−170 °C; ^{1}H NMR (500.13 MHz, $CDCl_3$): δ 0.38 (t, J = 7.0 Hz, 6 H), 2.03 (q, J = 7.0 Hz, 4 H), 6.22 (d, J = 8.0 Hz, 2 H), 6.79−6.85 (m, 4 H), 7.02 (d, J = 7.5 Hz, 2 H), 7.35−7.38 (m, 2 H), 7.51−7.53 (m, 2 H), 7.62 (d, J = 8.0 Hz, 1 H), 7.92 (d, J = 7.5 Hz, 1 H). ^{13}C NMR (125.77 MHz, $CDCl_3$): δ 152.62, 152.53, 144.46, 140.61, 140.02, 139.63, 130.36, 130.13, 126.89, 126.74, 126.42, 125.74, 122.43, 121.76, 121.34, 119.75, 115.62, 56.81, 32.68, 8.58. HRMS (ESI, m/z): $[M]^+$ calcd. for $C_{29}H_{24}BrNS$: 497.0807; found: 497.0801.

5-(9,9-Diethyl-7-(10H-phenothiazin-10-yl)-9H-fluoren-2-yl)-thiophene-2-carbaldehyde, ***3a***. A mixture of (5-(1,3-dioxolan-2-yl)thiophen-2-yl)tributylstannane (1.2 mmol), **2** (0.50 g, 1.0 mmol), and dry DMF (4 mL) was maintained at nitrogen atmosphere. After the addition of $Pd(PPh_3)_2Cl_2$ (7.0 mg, 1 mol %), it was heated at 80 °C for 24 h. On completion of the reaction, the mixture was poured into water and extracted with dichloromethane. The organic layer was washed with brine solution followed by water and dried over anhydrous Na_2SO_4. The volatiles were removed to obtain a solid residue. It was dissolved in glacial acetic acid (5 mL) and heated to 60 °C. After 30 min, it was treated with 10 mL of water and the heating continued for a further 6 h. The cooled solution was extracted with dichloromethane. The dichloromethane layer was washed liberally with water and dried over anhydrous Na_2SO_4. On removal of solvent, the obtained dark residue was purified by column chromatography on silica gel using hexane/dichloromethane (1:1) as eluant. Orange solid; yield 0.32 g (60%). mp 196−198 °C; IR (KBr, cm^{-1}) 1660 ($\nu_{C=O}$); ^{1}H NMR (500.13 MHz, $CDCl_3$): δ 0.38−0.43 (m, 6 H), 2.06−2.12 (m, 4 H), 6.24 (dd, J = 8.0 Hz, 1.5 Hz, 2 H), 7.80−7.86 (m, 4 H), 7.02−7.04 (m, 2 H), 7.38−7.40 (m, 2 H), 7.50 (d, J = 3.5 Hz, 1 H), 7.66 (d, J = 1.0 Hz, 1 H), 7.72−7.74 (m, 1 H), 7.78 (d, J = 4.0 Hz, 1 H), 7.81 (d, J = 8.0 Hz, 1 H), 7.95 (dd, J = 8.0 Hz, 0.5 Hz, 1 H), 9.92 (s, 1 H). ^{13}C NMR (125.77 MHz, $CDCl_3$): δ 182.76, 154.77, 153.30, 151.50, 144.44, 142.22, 142.11, 140.62, 140.31, 137.51, 132.22, 130.13, 126.91, 126.76, 125.86, 125.76, 124.06, 122.47, 122.07, 120.80, 120.67, 119.84, 115.69, 56.74, 32.74, 8.65, 8.57. HRMS (ESI, m/z): $[M]^+$ calcd. for $C_{38}H_{29}NOS_3$: 529.1529; found: 529.1520.

5′-(9,9-Diethyl-7-(10H-phenothiazin-10-yl)-9H-fluoren-2-yl)-[2,2′-bithiophene]-5-carbaldehyde, ***3b***. It was obtained from (5′-(1,3-dioxolan-2-yl)-2,2′-bithiophen-5-yl)tributylstannane (1.2 mmol) and **2** (0.50 g, 1.0 mmol) by following a procedure described above for **3a**. Red-orange solid; yield 0.35 g (58%). mp 236−238 °C; IR (KBr, cm^{-1}) 1665 ($\nu_{C=O}$); ^{1}H NMR (500.13 MHz, $CDCl_3$): δ 0.41 (t, J = 7.5 Hz, 6 H), 2.08−2.12 (m, 4 H), 6.24 (dd, J = 8.0 Hz, 1.5 Hz, 2 H), 6.80−6.86 (m, 4 H), 7.03 (dd, J = 7.5 Hz, 2.0 Hz, 2 H), 7.30 (d, J = 3.5 Hz, 1 H), 7.37−7.39 (m, 4 H), 7.59 (d, J = 1.5 Hz, 1 H), 7.66 (dd, J = 8.0 Hz, 1.5 Hz, 1 H), 7.70 (d, J = 4.0 Hz, 1 H), 7.78 (d, J = 8.0 Hz, 1 H), 7.93 (d, J = 8.0 Hz, 1 H), 9.88 (s, 1 H). ^{13}C NMR (125.77 MHz, $CDCl_3$): δ 182.73, 154.74, 153.27, 151.47, 148.44, 144.41, 142.19, 142.08, 140.59, 140.28, 138.86, 137.48, 135.94, 134.80, 133.21, 132.26, 130.09, 129.22, 128.58, 126.87, 126.73, 125.83, 125.73, 124.03, 122.43, 122.04, 120.76, 119.81, 115.66, 56.70, 32.70, 8.62. HRMS (ESI, m/z): $[M]^+$ calcd. for $C_{34}H_{27}NOS_2$: 611.1406; found: 611.1405.

4-(9,9-Diethyl-7-(10H-phenothiazin-10-yl)-9H-fluoren-2-yl)-benzaldehyde, ***3c***. A mixture of 4-formylphenylboronic acid (0.090 g, 0.6 mmol), **2** (0.250 g, 0.5 mmol), and K_2CO_3 (0.21 g) in THF/water (4:1) (20 mL) was maintained at nitrogen atmosphere. After the addition of $Pd(PPh_3)_4$ (17 mg, 3 mol %), it was heated at 80 °C for 12 h. On completion of the reaction, the mixture was poured into water and extracted with dichloromethane. The organic layer was washed with brine solution followed by water and dried over anhydrous Na_2SO_4. The volatiles were removed to obtain a solid residue, which was purified by column chromatography on silica gel using hexane/dichloromethane (1:1) as eluant. Yellow solid; yield 0.175 g (67%). mp 200−202 °C; IR (KBr, cm^{-1}) 1662 ($\nu_{C=O}$); ^{1}H NMR (500.13 MHz, $CDCl_3$): δ 0.49 (t, J = 7.5 Hz, 6 H), 2.09−2.17 (m, 4 H), 7.31 (pent, J = 4.0 Hz, 2 H), 7.44−7.47 (m, 4 H), 7.55−7.59 (m, 2 H), 7.65 (d, J = 1.5 Hz, 1 H), 7.69−7.71 (m, 1 H), 7.86−7.89 (m, 3 H), 7.96−8.01 (m, 3 H), 8.18 (d, J = 7.5 Hz, 2 H), 10.09 (s, 1 H). ^{13}C NMR (125.77 MHz, $CDCl_3$): δ 190.90, 151.16, 150.10, 146.43, 140.21, 139.97, 139.02, 137.82, 135.79, 134.07, 129.30, 126.67, 125.66, 125.63, 124.96, 122.35, 120.81, 120.79, 119.36, 118.90, 108.69, 55.60, 31.76, 7.68. HRMS (ESI, m/z): $[M]^+$ calcd. for $C_{36}H_{29}NOS$: 523.1965; found: 523.1953.

(E)-2-Cyano-3-(5-(9,9-diethyl-7-(10H-phenothiazin-10-yl)-9H-fluoren-2-yl)thiophen-2-yl)acrylic acid, ***4a***. A mixture of 5-(9,9-diethyl-7-(10*H*-phenothiazin-10-yl)-9*H*-fluoren-2-yl)thiophene-2-carbaldehyde (0.10 g, 0.19 mmol) (**3a**), cyanoacetic acid (0.022 g, 0.26 mmol), acetic acid (5 mL), and ammonium acetate (4 mg) was heated at 120 °C for 12 h. The resulting red solution was poured into ice-cold water to produce a red precipitate. This was filtered and washed thoroughly with water and dried. The solid was further crystallized from hot chloroform. Red solid; yield 0.091 g (80%). mp 266−268 °C; IR (KBr, cm^{-1}) 2202 ($\nu_{C\equiv N}$); ^{1}H NMR (500.13 MHz, DMSO-d_6): δ 0.29 (t, J = 7.5 Hz, 6 H), 2.14 (q, J = 7.0 Hz, 4 H), 6.18 (d, J = 8.0 Hz, 2 H), 6.84−6.86 (m, 2 H), 6.91−6.94 (m, 2 H), 7.07 (dd, J = 7.5 Hz, 1.5 Hz, 2 H), 7.41 (dd, J = 8.0 Hz, 1.5 Hz, 1 H), 7.54 (d, J = 1.5 Hz, 1 H), 7.84 (dd, J = 8.0 Hz, 1.5 Hz, 1 H), 7.90 (d, J = 4.0 Hz, 1 H), 7.94 (s, 1 H), 8.03−8.06 (m, 2 H), 8.18 (d, J = 8.0 Hz, 1 H), 8.51 (s, 1 H). ^{13}C NMR (125.77 MHz, DMSO-d_6): δ 153.00, 151.21, 146.69, 143.74, 141.64, 141.31, 140.22, 139.68, 138.16, 134.56, 133.99, 131.70, 129.73, 127.28, 126.61, 125.83, 125.37, 122.64, 121.21, 120.49, 118.83, 116.65, 115.53, 56.44, 31.55, 8.47. HRMS (ESI, m/z): $[M]^+$ calcd. for $C_{37}H_{28}N_2O_2S_2$: 596.1587; found: 596.1580.

(E)-2-Cyano-3-(5′-(9,9-diethyl-7-(10H-phenothiazin-10-yl)-9H-fluoren-2-yl)-[2,2′-bithiophen]-5-yl)acrylic acid, ***4b***. It was obtained from **3b** (0.12 g, 0.19 mmol) by following a procedure described above for **4a**. Red-orange solid; yield 0.108 g (84%). mp 276−278 °C; IR (KBr, cm^{-1}) 2208 ($\nu_{C\equiv N}$); ^{1}H NMR (500.13 MHz, DMSO-d_6): δ 0.27−0.33 (m, 6 H), 2.11−2.17 (m, 4 H), 6.17 (d, J = 8.0 Hz, 2 H), 6.83−6.89 (m, 4 H), 7.07 (d, J = 7.5 Hz, 2 H), 7.30 (d, J = 3.5 Hz, 1 H), 7.39 (d, J = 8.0 Hz, 1 H), 7.52 (s, 1 H), 7.65−7.70 (m, 1 H), 7.76−7.81 (m, 2 H), 7.88 (s, 1 H), 7.98−8.02 (m, 1 H), 8.14 (d, J = 8.0 Hz, 1 H), 8.50 (s, 1 H). ^{13}C NMR (125.77 MHz, DMSO-d_6): δ 152.85, 145.52, 143.78, 141.64, 140.51, 139.29, 138.14, 135.78, 133.98, 132.33, 129.69, 128.40, 127.27, 126.59, 125.70, 125.35, 124.91, 122.58, 122.37, 121.01, 119.93, 118.73, 116.71, 115.46, 56.37, 31.57, 8.48. HRMS (ESI, m/z): $[M]^+$ calcd. for $C_{41}H_{30}N_2O_2S_3$: 678.1464; found: 678.1456.

(E)-2-Cyano-3-(4-(9,9-diethyl-7-(10H-phenothiazin-10-yl)-9H-fluoren-2-yl)phenyl)acrylic acid, ***4c***. It was obtained from **3c** (0.10 g, 0.19 mmol) by following the procedure described above for **4a**. Yellow solid; yield 0.085 g (75%). mp 256−258 °C; IR (KBr, cm^{-1}) 2210 ($\nu_{C\equiv N}$); ^{1}H NMR (500.13 MHz, DMSO-d_6): δ 0.30 (t, J = 7.0 Hz, 6

DOI: 10.1021/am506149q
ACS Appl. Mater. Interfaces 2015, 7, 2249−2262

H), 2.10−2.19 (m, 4 H), 6.91−6.94 (m, 2 H), 7.07 (d, J = 7.5 Hz, 2 H), 7.41 (d, J = 7.5 Hz, 1 H), 7.54 (s, 4 H), 7.88 (d, J = 7.5 Hz, 1 H), 7.97 (s, 1 H), 8.05 (d, J = 8.5 Hz, 3 H), 8.18 (d, J = 8.5 Hz, 3 H), 8.39 (s, 1 H). ^{13}C NMR (125.77 MHz, DMSO-d_6): δ 159.26, 153.06, 151.02, 143.79, 140.66, 139.36, 137.83, 133.51, 132.86, 131.38, 130.48, 129.65, 128.75, 128.55, 127.38, 127.28, 126.86, 126.60, 126.27, 125.39, 122.60, 121.47, 120.89, 118.75, 115.48, 105.47, 56.37, 31.57, 8.51. HRMS (ESI, m/z): $[M + Na]^+$ calcd. for $C_{39}H_{30}N_2NaO_2S$: 613.1920; found: 613.1920.

3-(7-Bromo-9,9-diethyl-9H-fluoren-2-yl)-10-butyl-10H-phenothiazine, ***5***. A mixture of 10-butyl-10*H*-phenothiazin-3-ylboronic acid (0.40 g, 1.3 mmol), 2,7-dibromo-9,9-diethyl-9*H*-fluorene (0.98 g, 2.6 mmol), K_2CO_3 (0.27 g) in THF/water (4:1) (20 mL) was maintained at nitrogen atmosphere. After the addition of $Pd(PPh_3)_4$ (75 mg, 5 mol %), it was heated at 80 °C for 12 h. On completion of the reaction, the mixture was poured into water and extracted with dichloromethane. The organic layer was washed with brine solution followed by water and dried over anhydrous Na_2SO_4. The volatiles were removed to obtain a solid residue, which was purified by column chromatography on silica gel using hexane/dichloromethane (1:1) as eluant. Green-yellow solid; yield 0.43 g (60%). mp 72−74 °C; ^{1}H NMR (500.13 MHz, $CDCl_3$): δ 0.35 (t, J = 7.5 Hz, 6 H), 0.97 (t, J = 8.5 Hz, 3 H), 1.49 (quad, J = 7.5 Hz, 2 H), 1.79−1.87 (m, 2 H), 2.00−2.05 (m, 4 H), 3.88 (t, J = 7.0 Hz, 2 H), 6.83−6.96 (m, 2 H), 7.15−7.19 (m, 2 H), 7.41−7.51 (m, 7 H), 7.56 (d, J = 8.5 Hz, 1 H), 7.69 (d, J = 8.0 Hz, 6 H). ^{13}C NMR (125.77 MHz, $CDCl_3$): δ 147.05, 145.03, 142.59, 140.39, 139.62, 136.88, 135.37, 133.32, 132.00, 131.38, 128.47, 127.87, 126.30, 125.26, 124.17, 123.57, 123.27, 122.80, 121.22, 120.71, 120.50, 115.70, 115.27, 52.76, 47.39, 33.06, 27.12, 19.66, 13.32, 8.83. HRMS (ESI, m/z): $[M]^+$ calcd. for $C_{33}H_{32}BrNS$: 553.1434; found: 553.1424.

5-(7-(10-Butyl-10H-phenothiazin-3-yl)-9,9-diethyl-9H-fluoren-2-yl)thiophene-2-carbaldehyde, ***6a***. It was obtained from (5-(1,3-dioxolan-2-yl)thiophen-2-yl)tributylstannane (0.6 mmol) and **5** (0.27 g, 0.5 mmol) by following a procedure described above for **3a**. Orange-yellow solid; yield 0.17 g (58%). mp 150−152 °C; IR (KBr, cm^{-1}) 1665 ($\nu_{C=O}$); ^{1}H NMR (500.13 MHz, $CDCl_3$): δ 0.39 (t, J = 7.5 Hz, 6 H), 0.98 (t, J = 8.0 Hz, 3 H), 1.48−1.53 (m, 2 H), 1.82−1.88 (m, 2 H), 2.09 (quad, J = 7.0 Hz, 4 H), 3.91 (t, J = 7.0 Hz, 2 H), 6.14 (s, 1 H), 6.90−6.92 (m, 1 H), 6.94−6.96 (m, 1 H), 7.16−7.19 (m, 3 H), 7.26−7.27 (m, 1 H), 7.46−7.48 (m, 3 H), 7.52 (d, J = 8.0 Hz, 1 H), 7.56 (s, 1 H), 7.65 (d, J = 8.0 Hz, 1 H), 7.69−7.73 (m, 2 H), 9.92 (s, 1 H). ^{13}C NMR (125.77 MHz, $CDCl_3$): δ 182.49, 151.01, 150.82, 144.43, 144.26, 141.04, 140.44, 139.95, 139.11, 138.56, 136.12, 132.73, 127.51, 127.29, 127.05, 125.91, 125.78, 125.48, 124.92, 124.71, 123.51, 123.00, 122.41, 120.88, 120.09, 119.91, 115.55, 115.36, 56.31, 47.18, 32.86, 29.01, 20.23, 13.62, 8.63. HRMS (ESI, m/z): $[M]^+$ calcd. for $C_{38}H_{35}NOS_2$: 585.2155; found: 585.2150.

5′-(7-(10-Butyl-10H-phenothiazin-3-yl)-9,9-diethyl-9H-fluoren-2-yl)-[2,2′-bithiophene]-5-carbaldehyde, ***6b***. It was obtained from (5′-(1,3-dioxolan-2-yl)-2,2′-bithiophen-5-yl)tributylstannane (0.6 mmol) and **5** (0.27 g, 0.5 mmol) by following a procedure described above for **3a**. Orange solid; yield 0.18 g (54%). mp 158−160 °C; IR (KBr, cm^{-1}) 1660 ($\nu_{C=O}$); ^{1}H NMR (500.13 MHz, $CDCl_3$): δ 0.39 (t, J = 7.0 Hz, 6 H), 0.97 (t, J = 7.5 Hz, 3 H), 1.49 (quad, J = 7.5 Hz, 2 H), 1.81−1.87 (m, 2 H), 2.09 (quad, J = 7.0 Hz, 4 H), 3.90 (t, J = 7.0 Hz, 2 H), 6.89−6.93 (m, 1 H), 6.94−6.95 (m, 1 H), 7.09 (m, 1 H), 7.15−7.18 (m, 3 H), 7.28 (d, J = 4.0 Hz, 1 H), 7.46−7.47 (m, 2 H), 7.49 (s, 1 H), 7.51−7.53 (m, 1 H), 7.55 (s, 1 H), 7.58−7.60 (m, 1 H), 7.69−7.73 (m, 2 H), 9.87 (s, 1 H). ^{13}C NMR (125.77 MHz, $CDCl_3$): δ 182.62, 151.17, 150.99, 145.33, 144.60, 144.42, 141.20, 140.61, 139.23, 138.72, 136.26, 135.93, 132.86, 127.64, 127.45, 126.07, 125.44, 125.64, 125.05, 124.86, 124.58, 123.68, 123.14, 122.56, 121.02, 120.24, 120.18, 120.05, 115.69, 115.51, 56.46, 47.33, 33.01, 27.02, 20.37, 13.80, 8.78. HRMS (ESI, m/z): $[M]^+$ calcd. for $C_{42}H_{37}NOS_3$: 667.2032; found: 667.2029.

(E)-3-(5-(7-(10-Butyl-10H-phenothiazin-3-yl)-9,9-diethyl-9H-fluoren-2-yl)thiophen-2-yl)-2-cyanoacrylic acid, ***7a***. It was obtained from **6a** (0.117 g, 0.20 mmol) by following a procedure described above for **4a**. Red-orange solid; yield 0.97 g (74%). mp 180−182 °C; IR (KBr, cm^{-1}) 2210 ($\nu_{C\equiv N}$); ^{1}H NMR (500.13 MHz, $CDCl_3$): δ 0.36−0.41 (m, 6 H), 0.93−0.98 (m, 3 H), 1.49 (quad, J = 7.5 Hz, 2 H), 1.82−1.85 (m, 2 H), 2.09−2.14 (m, 4 H), 3.90 (t, J = 7.0 Hz, 2 H), 6.89−6.91 (m, 1 H), 6.93−6.95 (m, 1 H), 7.16 (d, J = 7.5 Hz, 1 H), 7.49−7.55 (m, 5 H), 7.61−7.66 (m, 2 H), 7.71−7.77 (m, 4 H), 7.95−7.99 (m, 1 H), 7.69−8.37 (s, 1 H). ^{13}C NMR (125.77 MHz, $CDCl_3$): δ 161.92, 151.14, 150.14, 148.60, 147.01, 145.08, 142.88, 142.63, 140.93, 139.73, 136.96, 135.41, 133.36, 131.94, 131.43, 128.51, 127.92, 126.26, 125.84, 125.34, 125.26, 124.21, 123.62, 123.31, 122.85, 121.28, 120.99, 120.77, 120.50, 115.64, 115.23, 52.50, 47.18, 32.82, 27.32, 19.10, 13.75, 8.71. HRMS (ESI, m/z): $[M]^+$ calcd. for $C_{41}H_{36}N_2O_2S_2$: 652.2213; found: 652.2210.

(E)-3-(5′-(7-(10-Butyl-10H-phenothiazin-3-yl)-9,9-diethyl-9H-fluoren-2-yl)-[2,2′-bithiophen]-5-yl)-2-cyanoacrylic acid, ***7b***. It was obtained from **6b** (0.134 g, 0.20 mmol) by following a procedure described above for **4a**. Red solid; yield 0.118 g (80%); mp 193−195 °C; IR (KBr, cm^{-1}) 2211 ($\nu_{C\equiv N}$); ^{1}H NMR (500.13 MHz, $CDCl_3$): δ 0.39 (t, J = 7.5 Hz, 6 H), 0.96−0.98 (m, 3 H), 1.49 (quad, J = 7.5 Hz, 2 H), 1.84 (t, J = 7.0 Hz, 2 H), 2.09 (quad, J = 7.0 Hz, 4H), 3.90 (t, J = 7.0 Hz, 2 H), 6.89−6.92 (m, 1 H), 6.93−6.95 (m, 2 H), 7.16 (d, J = 7.5 Hz, 2 H), 7.29 (d, J = 4.0 Hz, 1 H), 7.36 (d, J = 3.5 Hz, 1 H), 7.41 (d, J = 4.0 Hz, 1 H), 7.45−7.47 (m, 2 H), 7.48 (s, 1 H), 7.53 (dd, J = 8.0 Hz, 1.5 Hz, 1 H), 7.57 (s, 1 H), 7.62 (dd, J = 8.0 Hz, 1.5 Hz, 1 H), 7.68−7.69 (m, 1 H), 7.71−7.74 (m, 2 H), 8.30 (s, 1 H). ^{13}C NMR (125.77 MHz, $CDCl_3$): δ 159.89, 151.23, 150.93, 145.16, 144.51, 143.28, 141.81, 139.74, 139.39, 138.30, 135.69, 134.44, 134.41, 132.09, 127.48, 127.29, 125.80, 125.55, 125.34, 124.94, 124.43, 124.11, 122.43, 120.89, 120.13, 115.52, 115.38, 56.43, 47.30, 32.88, 29.74, 20.20, 13.80, 8.63. HRMS (ESI, m/z): $[M]^+$ calcd. for $C_{45}H_{38}N_2O_2S_3$: 734.2090; found: 734.2080.

Computational Methods. All the computations were performed with the Gaussian 09 program[35] package in a computer workstation. The ground-state geometries were fully optimized without any symmetry constraints at the density functional theory (DFT) level with Becke's three parameters hybrid functional[36] and Lee et al.'s correlational functional (B3LYP)[37] using 6-31G(D,P) basis set on all atoms. The default parameters for the convergence criteria were used. Vibrational analyses on the optimized structures were performed to confirm the structure. No negative frequency vibrations were observed for the optimized geometries. The excitation energies and oscillator strengths for the lowest 10 singlet transitions for the optimized geometry in the ground state were obtained by time-dependent density functional theory (TDDFT) calculations using the same basis set.

X-ray Crystal Structure Determination. Crystals of the compounds **4c** suitable for X-ray data collection were grown from dimethyl sulfoxide solution. X-ray data of **4c** was collected on a CCD diffractometer using Mo Kα (λ = 0.71073). The data were corrected for Lorentz and polarization effects. A total of 14 350 reflections were measured out of which 5121 were independent and 2023 were observed [$I > 2\ \sigma(I)$] for maximum theta 26.56° at room temperature. The structures were solved by direct methods using SHELXS-97[38] and refined by full-matrix least-squares refinement methods based on F^2, using SHELXL-97.[39] All non-hydrogen atoms were refined anisotropically. All hydrogen atoms were fixed geometrically with their U_{iso} values 1.2 times of the phenylene and methylene carbons and 1.5 times of the methyl carbons. All calculations were performed using WinGX package.[40] A final refinement of 438 parameters gave R_1 = 0.0719 and wR_2 = 0.1901 for the observed data and R_1 = 0.2062 and wR_2 = 0.2585 for all data. The relatively high R-values are due to the poor diffraction of crystals.

DSSC Fabrication and Characterization. The DSSCs were fabricated and characterized by following the procedures detailed in our earlier publication. A fluorine-doped SnO_2 conducting glass (FTO, 7 X sq^{-1}, transmittance ~80%) was first cleaned with a neutral cleaner and then washed with deionized water, acetone, and isopropyl alcohol, sequentially. The conducting surface of the FTO was treated with a solution of titanium tetraisopropoxide (1 g) in 2-methoxyethanol (3 g) to obtain a good mechanical contact between the conducting glass and TiO_2 film, as well as to isolate the conducting glass surface from the electrolyte. TiO_2 pastes were coated onto the treated conducting glass

DOI: 10.1021/am506149q
ACS Appl. Mater. Interfaces 2015, 7, 2249−2262

Scheme 1. Synthesis of the T-Shaped Dyes

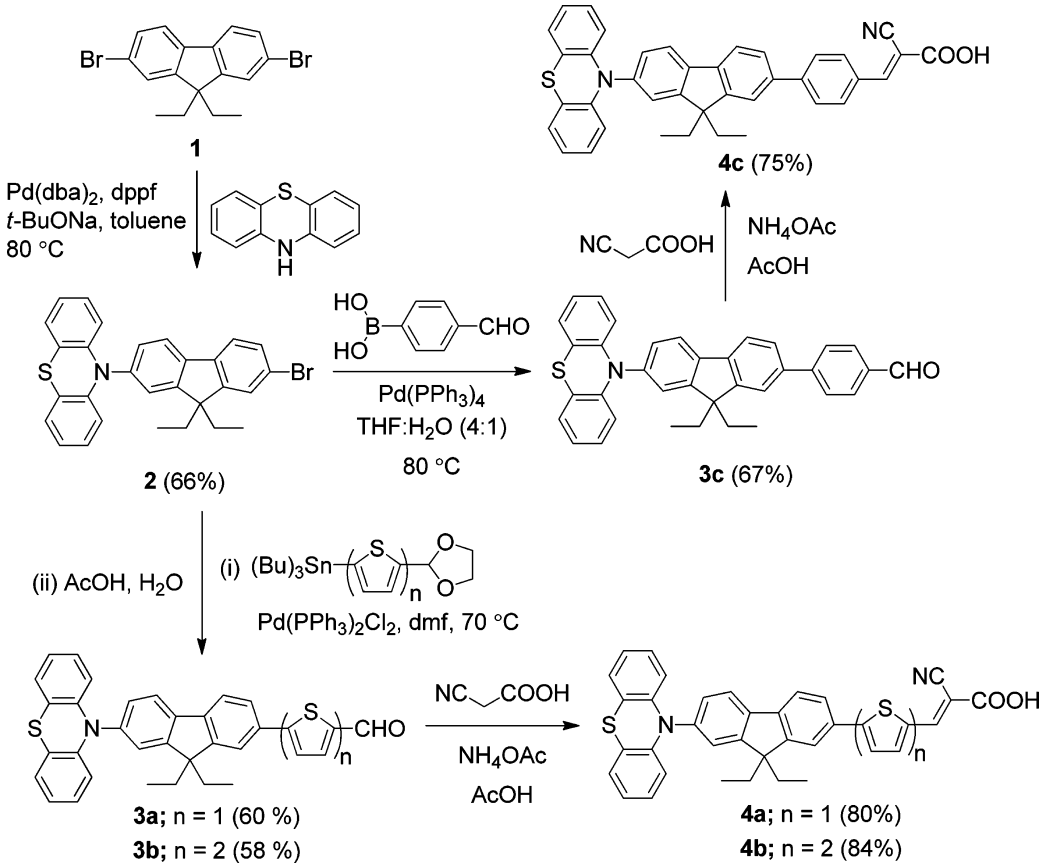

by using the doctor blade technique. To coat each TiO_2 layer, the dried TiO_2 film was gradually heated to 450 °C in an oxygen atmosphere and subsequently sintered at that temperature for 30 min. The TiO_2 photoanodes of the DSSCs employed in the experiments were composed of a 12 μm thick transparent TiO_2 (20 nm) layer and a scattering TiO_2 (300 nm) layer of 4 μm thickness. After sintering at 450 °C and cooling to 80 °C, the TiO_2 film was immersed in a ~3 × 10^{-4} M solution of dye at room temperature for 24 h. For the coadsorbed solar cells, dye bath solutions containing chenodeoxycholic acid (CDCA) (1 and 2 mM) were used. Various organic dye solutions were prepared in a mixing solvent containing ACN, *tert*-butyl alcohol, and dimethyl sulfoxide (DMSO) (volume ratio of 3.5:3.5:3). The thus prepared TiO_2/dye electrode was placed on a platinum-sputtered conducting glass electrode (ITO, 7 X sq^{-1}), keeping the two electrodes separated by a 25 μm thick Surlyn. The two electrodes were then sealed by heating. The electrolyte was composed of 0.1 M LiI, 0.6 M 1-propyl-2,3-dimethylimidazolium iodide (DMPII), 0.05 M I_2, and 0.5 M *tert*-butylpyridine (TBP) in a solvent mixture of acetonitrile(ACN)/3-methoxypropionitrile (MPN) with a volume ratio of 1:1. The electrolyte was injected into the gap between the electrodes by capillarity; the electrolyte-injecting hole was previously made in the counter electrode with a drilling machine, and the hole was sealed with hot-melt glue after the injection of the electrolyte.

The surface of the DSSC was covered by a mask with a light-illuminated area of 0.16 cm^2 and then illuminated by a class A quality solar simulator (XES-301S, AM1.5G, San-Ei Electric Co., Ltd.). Incident light intensity (100 mW cm^{-2}) was calibrated with a standard silicon cell (PECSI01, Peccell Technologies, Inc.). Photocurrent–voltage curves of the DSSCs were obtained with a potentiostat/galvanostat (PGSTAT30, Autolab, Eco-Chemie, Netherlands). The thickness of the TiO_2 film was judged by scanning electron microscopic images (SEM). For UV absorption spectra, dye molecules were coated on the TiO_2 films, and the corresponding spectra were obtained using a JASCO UV–vis spectrophotometer equipped with an integrating sphere. The baseline was corrected with a bare TiO_2 coated FTO substrate. Electrochemical impedance spectra (EIS) were obtained from the potentiostat/galvanostat, equipped with a FRA2module, under a constant light illumination of 100 mW cm^{-2}. The frequency range explored was 10–65 kHz. The applied bias voltage was set at the open-circuit voltage of the DSSC between the ITO-Pt counter electrode and the FTO-TiO_2 dye working electrode, starting from the short-circuit condition; the corresponding AC amplitude was 10 mV. The impedance spectra were analyzed using an equivalent circuit model. Incident photocurrent conversion efficiency (IPCE) curves were obtained under short-circuit conditions. The light source was a class A quality solar simulator (PEC-L11, AM 1.5 G); light was focused through a monochromator onto the photovoltaic cell. The monochromator was incremented through the visible spectrum to generate the IPCE (λ) as defined by IPCE (λ) = 1240 ($J_{SC}/\lambda\varphi$), where λ is the wavelength, J_{SC} is the short-circuit photocurrent density (mA cm^{-2}) recorded with a potentiostat/galvanostat, and φ is the incident radiative flux (Wm^{-2}) measured with an optical detector and a power meter.

RESULTS AND DISCUSSION

Synthesis and Characterization. Syntheses of the sensitizers (**4** and **7**) are shown in Scheme 1. In general, the dyes were prepared by a three-step protocol. For the type I dyes, in the first step (Scheme 1), the stoichiometrically controlled C–N cross-coupling reaction[41] between 2,7-dibromo-9,9-diethylfluorene (**1**) and 10*H*-phenothiazine was used to obtain the monosubstituted intermediate (**2**), while for type 2 sensitizers a stoichiometrically controlled Suzuki cross coupling reaction[42] between 2,7-dibromo-9,9-diethylfluorene and 10-butyl-10*H*-phenothiazin-3-ylboronic acid produced the desired monosubstituted intermediate, **5** (Scheme 2). Then, the

DOI: 10.1021/am506149q
ACS Appl. Mater. Interfaces 2015, 7, 2249–2262

Scheme 2. Synthesis of the Rod-Like Dyes

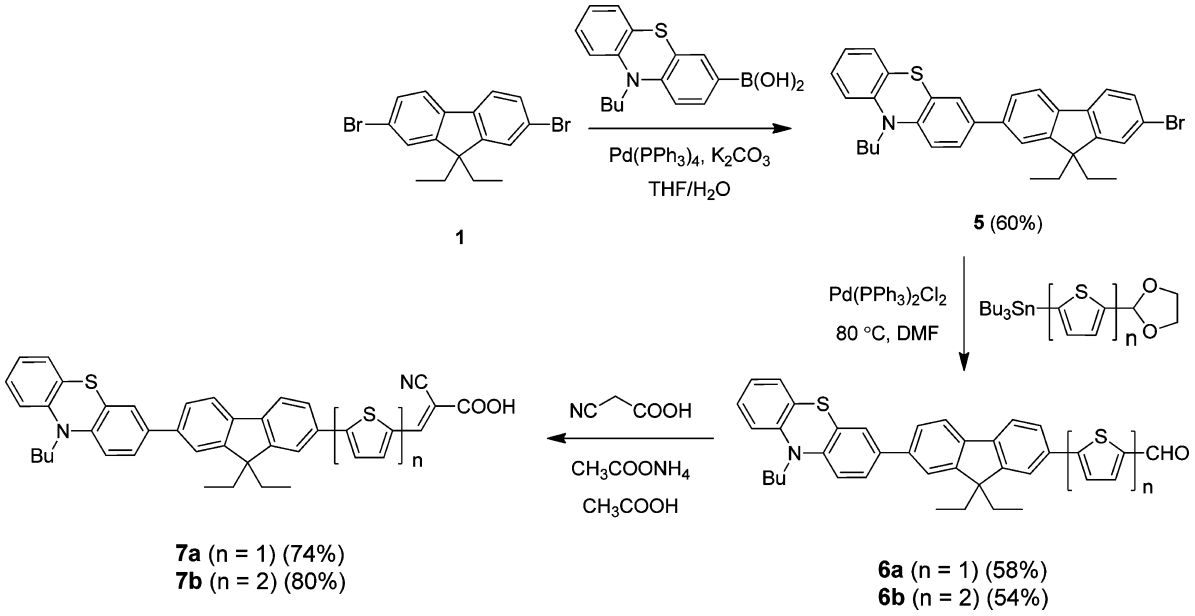

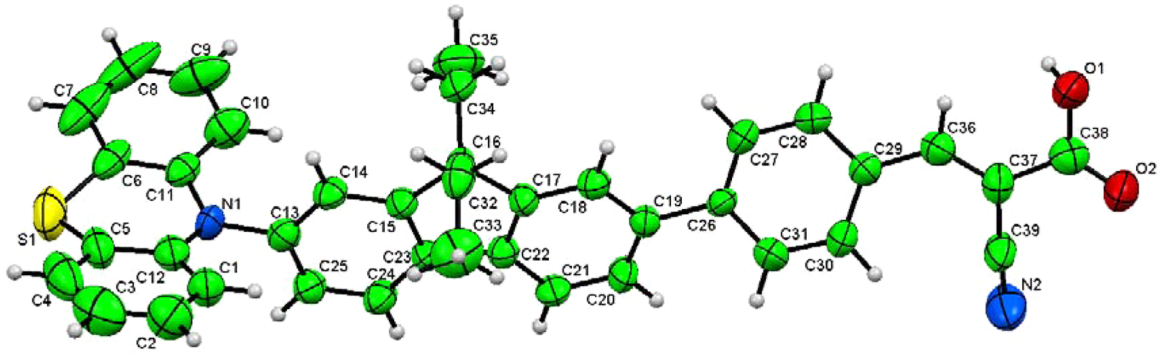

Figure 2. ORTEP plot (50% thermal ellipsoids) of the dye **4c**.

aldehydes (**3** and **6**) were synthesized by treating the aryl bromides (**2** and **5**) with corresponding boron or tin derivatives by following Suzuki or Stille reaction[43] conditions and subsequent acid hydrolysis. Finally, the dyes (**4** and **7**) were generated by Knoevenagel condensation of cyanoacetic acid with the aldehydes (**3** and **6**) in the presence of ammonium acetate.

The structure of the dye **4c** was also confirmed by single crystal X-ray diffraction analysis (Figure 2). The compound crystallizes in the triclinic space group *P*-1 with a = 9.4861(15) A°, b = 13.822(2) A°, c = 14.253(3) A°; α = 100.383(7)°, β = 90.419(8)°, and γ = 107.068(6)°; Z = 2. The C5−S1−C6 and C11−N1−C12 bond angles of the compound are 101.4(4)° and 123.5(6)°, respectively. The folding angle between the least-squares planes of two phenyl ring in phenothiazine is 161.41°. The phenothiazine unit is almost perpendicular (dihedral angle between the planes = 89.34°) to fluorene moiety while the phenyl ring is twisted by 35.36°. Such kind of twisting in the linker is found to be useful in decelerating the charge recombination in the charge separated states.

The remarkable feature of the crystal packing is the presence of four types of weak interactions, H···H, C···H, H···N, and S···S (Figure 3). Due to the weak intermolecular interaction (C21···H1A = 2.869 A°) between two neighboring molecules, they are arranged in dimeric fashion.[44] The molecules in the dimers adopt antiparallel arrangement due to the alkyl chains present in the fluorene nucleus and display slipped stacking motifs. For slip-stacks, in a column of dimers, the distance between the two molecular dimers is 18.282 A°. It appears more reasonable to describe the closely spaced dimer in the framework of weak *J*-aggregate formation. Further, short S···S (3.379 A°) contacts are found between the neighboring columns in its crystals, which drives the formation of ideal face-to-face molecular stacking. It is well-known that *J*-aggregate formation is one of the important factors for the incident photon to energy conversion efficiency (IPCE) in DSSC.[45] In another direction, weak intermolecular interaction (H14···C7 = 2.843 A° and H14···C7 = 2.366 A°) between the fluorene unit of one molecule and phenothiazine moiety of another molecules gives rise to an inverted cofacial pair. It is noted that cofacial arrangement promotes effective overlap of orbitals and endorses carrier hooping between the molecules.[46] With respect to the five-membered ring in the fluorene residue, the ethyl substituents are virtually perpendicular which is evident from the torsion angles of C17−C16−C32−C33 and C17−C16−C34−C35 segments (−58.0(8)° and 56.0(8)°, respectively).

Optical Properties. Absorption spectra of the dyes recorded in dichloromethane are displayed in Figure 4, and the pertinent data are listed in Table 1. Two distinctive bands

DOI: 10.1021/am506149q
ACS Appl. Mater. Interfaces 2015, 7, 2249−2262

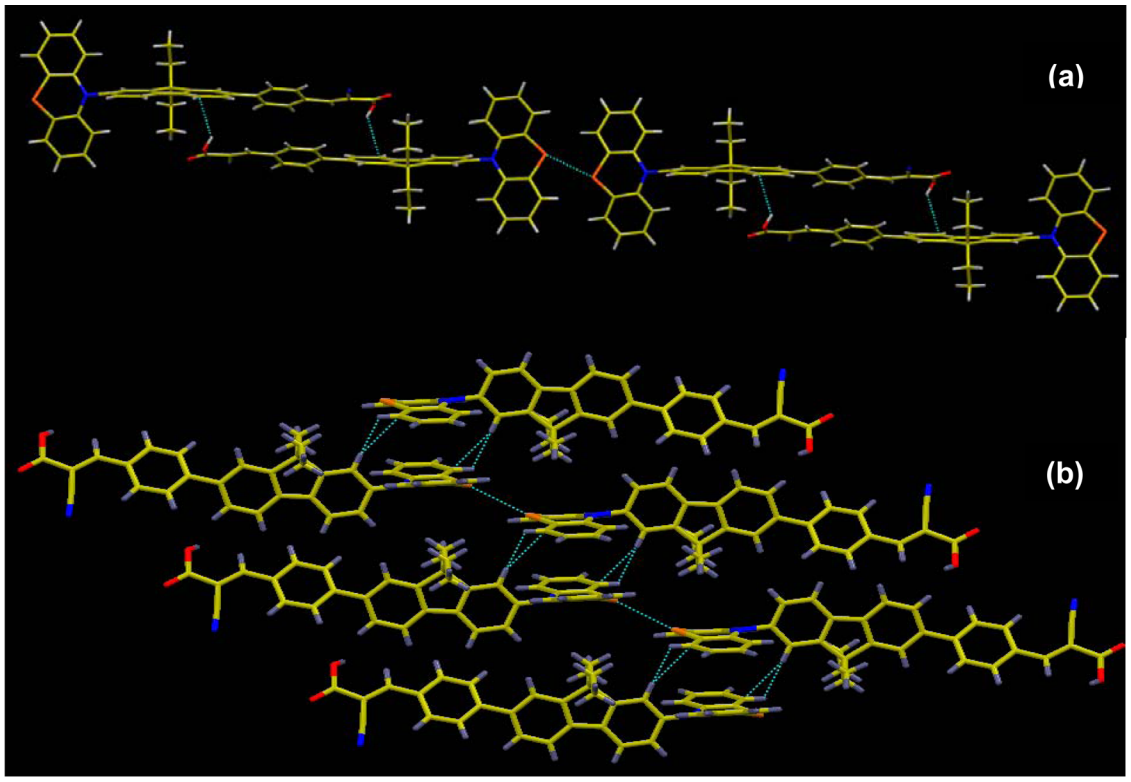

Figure 3. Packing modes in **4c** showing (a) C21···H1A and S···S interactions; (b) C7···H14 interactions.

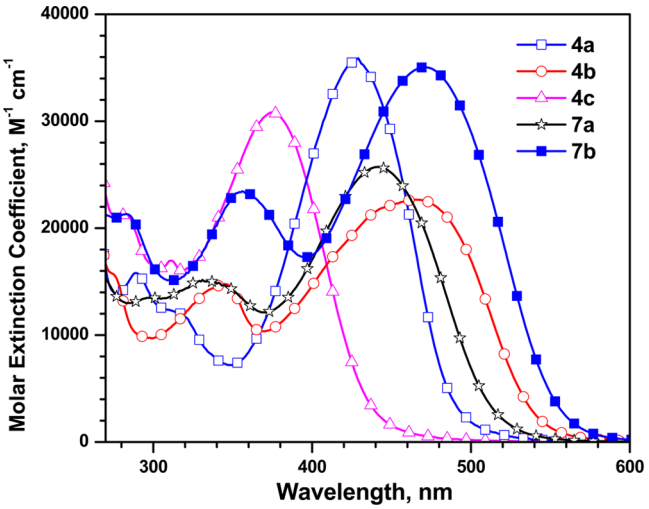

Figure 4. Absorption spectra of the dyes recorded in DCM solutions.

are observed for the dyes. The band appearing at the longer wavelength region of 360−560 nm is mainly ascribed to the charge transfer (CT) from phenothiazine donor to cyanoacrylic acid acceptor. The second band, in the region of 280−350 nm, is originating from the phenothiazine and fluorene localized $\pi-\pi^*$ transitions.[23] The molar extinction coefficients of the charge transfer transition in these dyes are significantly larger than the ruthenium-based dyes.[2,3] Interestingly, the absorption maxima of rod-like dyes (**7**) are slightly red-shifted when compared to the analogous T-shaped dyes (**4**). This bathochromic shift probably points to the elongation of conjugation into the phenothiazine ring via the C3 carbon, while the electronic coupling between phenothiazine and the acceptor is poor in the T-shaped dyes due to the perpendicular orientation of the phenothiazine and conjugation pathway (*vide supra*). Also, the dyes (**4b** and **7b**) possessing bithiophene in the conjugation displayed slightly longer wavelength CT transition than the corresponding thiophene-containing dyes (**4a** and **7a**).[8,47] The dye possessing phenyl linker (**4c**) displayed the most blue-shifted absorption attributable to the

Table 1. Optical and Electrochemical Data of the Dyes

dye	λ_{abs},[a] nm (ε, $M^{-1}cm^{-1} \times 10^3$)	λ_{TiO_2}, nm	E_{ox}, mV (ΔE_p, mV)[b]	HOMO,[c] eV	LUMO,[d] eV	E_{0-0},[e] eV	E^*_{0-0},[f] V
4a	429 (35.9), 299 (15.8)	445	272 (73)	5.07	2.59	2.48	−1.43
4b	465 (22.7), 345 (14.8)	485	260 (100)	5.06	2.83	2.23	−1.20
4c	374 (30.8), 311 (16.9), 283 (21.3)	406	265 (48)	5.07	2.40	2.67	−1.64
7a	441 (25.7), 331 (15.2), 266 (15.8)	514	234 (67)	5.03	2.70	2.33	−1.33
7b	471 (35.1), 356 (23.5), 283 (21.3), 267 (21.4)	488	220 (55)	5.02	2.83	2.19	−1.20

[a] λ_{abs}: absorption maxima in dichloromethane solution. [b] Redox potentials are reported with reference to the ferrocene internal standard. [c] Deduced from the oxidation potential using the formula HOMO = 4.8 + E_{ox}. [d] Obtained from the optical band gap and the electrochemically deduced HOMO value. [e] Calculated from optical edge. [f] Excited-state oxidation potential versus NHE.

DOI: 10.1021/am506149q
ACS Appl. Mater. Interfaces 2015, 7, 2249−2262

twisting of the linker which hampers the donor−acceptor interaction.[30,48]

The role of the donor−acceptor interactions on the electronic spectra is clearly evident on comparing the absorption maxima of the parent bromo-derivatives (**2** and **5**) and the aldehydes (**3** and **6**) (Figure S1, Supporting Information) with that of the dyes (**4** and **7**). For a similar chromophore, the absorption wavelength shifts to the low energy region on introduction of aldehyde or cyanoacrylic acid segment in the dye. It is interesting to compare the absorption spectra of the dye **4a** and **7a** with the related dyes **D1** and **SH-7** reported in the literature.[21,19] The absorption maxima for the dye **4a** is bathochromically shifted when compared to the dye **D1** (380 nm), whereas the absorption maxima for the dye **7a** shows higher molar extinction coefficient than the dye **SH-7** (16.2×10^3, M^{-1} cm^{-1}). This clearly indicates that insertion of the fluorene segment improves the donor−acceptor interactions and consequently the light harvesting properties.

The absorption spectra of the dyes recorded on thin TiO_2 film are shown in Figure 5. The absorption maxima of the dyes

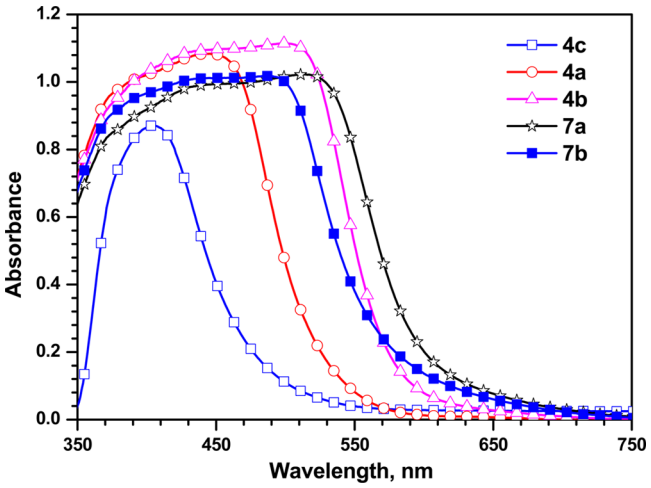

Figure 5. Absorption spectra of the dyes recorded on thin TiO_2 film.

on the TiO_2 film show broadening and a red-shift compared to that observed in solution. This may be due to *J*-aggregation of dyes at the TiO_2 surface.[49] Further, on addition of a small amount of trifluoroacetic acid or triethylamine to the dye, the solutions in DCM exhibited red- or blue-shift, respectively, for the absorption maxima (Figure 6, Table S1, Supporting Information). This indicates that the dyes are present in a partially deprotonated state in the solution; therefore, addition of trifluoroacetic acid (TFA) shifts the equilibrium toward the protonated form and tenders a red-shift in the absorption spectra, while the addition of triethylamine (TEA) shifts the equilibrium to the deprotonated form and causes a blue-shift.[50] A blue-shift in the absorption spectra of the dyes was observed when recorded in tetrahydrofuran (THF) or *N*,*N*-dimethylformamide (DMF) solutions (Figure 6). This is probably due to the chemical interaction of the solvent with the dyes. In THF, hydrogen bonding may reduce the acceptor strength of carboxylic acid unit while in DMF the equilibrium is probably shifted to the deprotonated form due to the basic nature of DMF.[51] Interestingly, in DMF, the absorption maxima of the dyes closely matched with those observed in the presence of TEA. It clearly indicates that the dyes are in the deprotonated state in DMF.

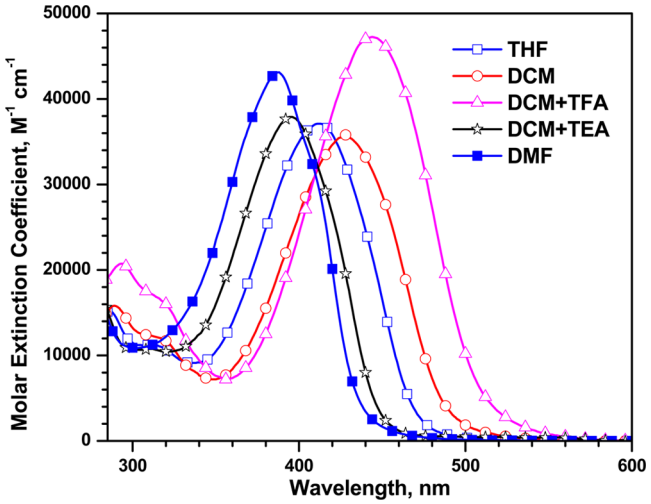

Figure 6. Absorption spectra of the dye **4a** recorded in different solvents.

Electrochemical Properties. The electrochemical properties of the dyes were investigated by using cyclic voltammetry to elucidate the thermodynamic driving force available for the electron injection and dye regeneration. All the dyes displayed one quasi reversible redox couple (Figure 7, Table 1)

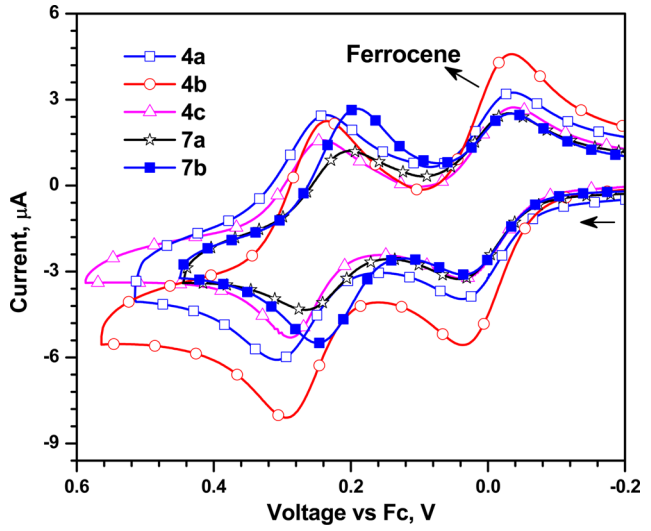

Figure 7. Cyclic voltammograms of the dyes recorded for DCM solutions.

attributable to the removal of electron from the phenothiazine unit. The rod-like dyes (**7**) displayed low oxidation potentials when compared to the corresponding T-shaped dyes (**4**). Easy oxidation of the dyes **7** suggests a comparatively more electron richness for these dyes. Similarly, low oxidation potential observed for **4c** when compared to **4a** is attributed to the nonplanarity of the phenyl linker which diminishes the donor−acceptor interactions and facilitates the electrochemical electron-removal from the donor. Also, within the class, the bithiophene dyes (**4b** and **7b**) displayed lower oxidation potentials than the respective monothiophene dyes (**4a** and **7a**) due to enhanced electron density in the bithiophene dyes.

To identify the feasibility of electron injection from the dye to TiO_2, we have estimated the excited-state redox potential (E^*_{ox}) of the sensitizers from the first oxidation potential (E_{ox}) at

DOI: 10.1021/am506149q
ACS Appl. Mater. Interfaces 2015, 7, 2249−2262

the ground state and the zero−zero electronic transition energy (E_{0-0}) from the following relation:

$$E_{ox}^{*} = E_{ox} - E_{0-0}$$

The optical band gap (E_{0-0}) was derived from the absorption edge. For an efficient electron injection from the excited dye to the TiO_2 electrode, the dyes must possess excited-state potentials lower than the conduction band edge energy. This will ensure an energetically favorable downhill electron injection. The E_{ox}^{*} values observed for the dyes (−1.20 to −1.64 V versus NHE) (Figure 8) are more negative than the

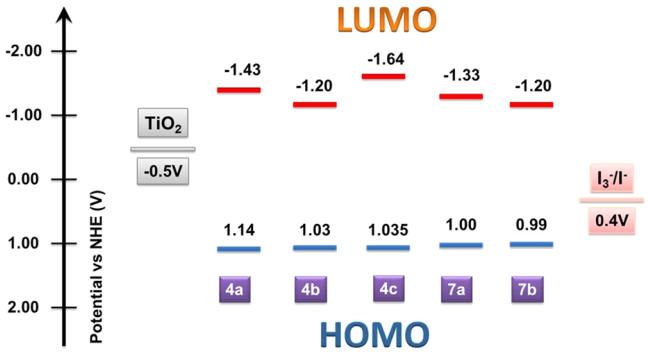

Figure 8. Energy level diagram of the dyes and related materials.

conduction band edge energy level of the TiO_2 electrode (−0.5 V vs NHE).[52] The dye regeneration is essential to achieve a high stability and operational lifetime for the DSSCs. Efficient dye regeneration is possible if the ground-state redox potential of the dye is more positive than that of the electrolyte redox potential. For the dyes reported here, the oxidation potentials lie in the range of 0.99−1.04 V vs NHE. These values are more positive than that of the electrolyte (I^-/I_3^-) redox couple (~0.4 V vs NHE)[53] and suggest facile dye regeneration with the selected electrolyte.

Theoretical Calculations. To understand the electronic structure of the dyes, the geometries of the dyes were optimized by density functional theory (DFT)[54] calculations at the 6-31+G(D,P) level using hybrid correlation functional B3LYP. The vertical excitation energies were computed using time-dependent density functional theory in the same level. The computed energies of the vertical excitations and their assignments are collected in Table S2, Supporting Information, and Figure 9 shows the electron distribution of the highest occupied molecular orbital (HOMO) and LUMO of the selected dyes. From the optimized geometries, it is clearly evident that the phenothiazine and fluorene units are perpendicular to one another in the T-shaped dyes while in the rod-like structures they are in a nearly coplanar arrangement. Among the T-shaped dyes, the variation of π-linker present between the fluorene and cyanoacrylic acid units affects the adsorption geometries on the TiO_2 surface. For instance, the presence of phenyl ring in the dye **4c** provides a stretched configuration as the distance between the phenothiazine nitrogen atom to carboxylic acid carbon of anchoring group is larger (16.4 A°) when compared with the dye **4a** having a thiophene ring (15.8 A°) (Figure S8, Supporting Information). Further, the presence of phenyl ring in **4c** significantly enlarges the dihedral angle between the fluorene unit and the π-spacer up to 35.70°, which is nearly 12° larger than that of the dye **4a** (23.94°). Both of these factors in the dye **4c** reduce the effective overlap of π-orbitals and increase the HOMO−LUMO energy gap among all the dyes which in turn corresponds well with the blue-shifted absorption spectra on TiO_2. For all the

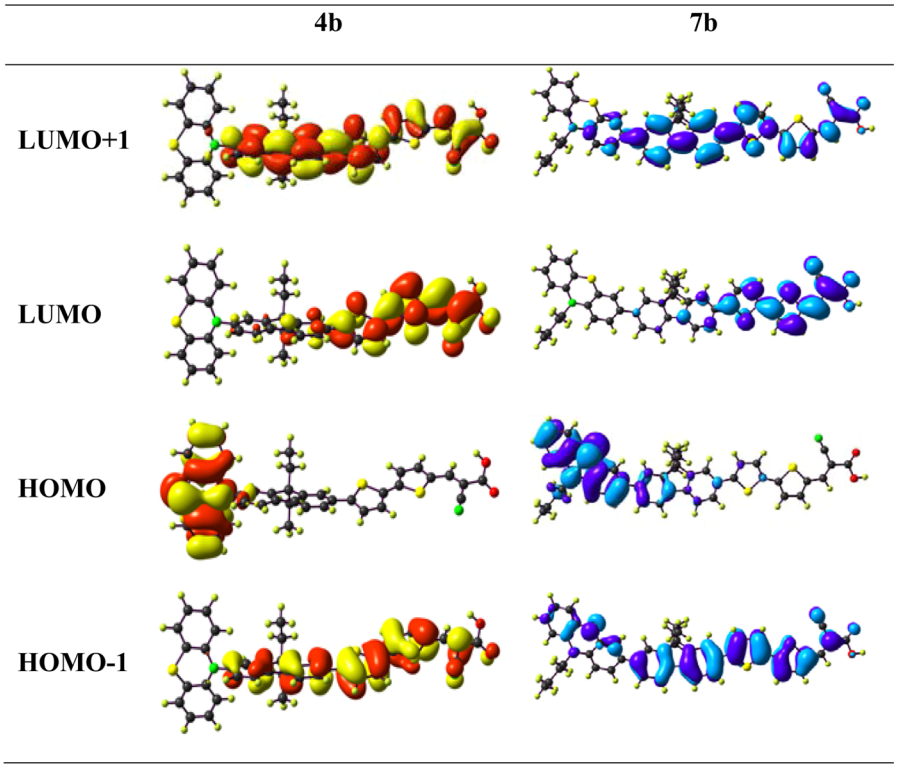

Figure 9. Electronic distribution in the frontier molecular orbitals of the dyes **4b** and **7b**.

DOI: 10.1021/am506149q
ACS Appl. Mater. Interfaces 2015, 7, 2249−2262

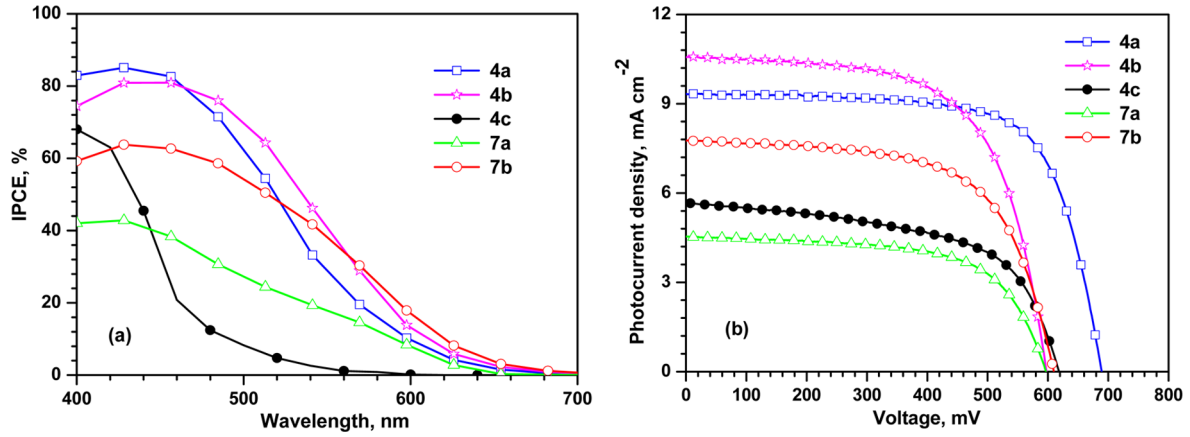

Figure 10. (a) IPCE and (b) *I*–*V* plots of the DSSCs fabricated using the dyes.

Table 2. Performance Parameters of the DSSC Devices Using the Dyes

dyes	η (%)	V_{OC} (mV)	J_{SC} (mA cm^{-2})	FF	R_{ct2} (ohm)	τ_e (ms)	R_{rec} (ohm)
4a	4.47 ± 0.09	690 ± 1.24	9.36 ± 0.06	0.69 ± 0.01	25.52	3.43	28.51
4b	4.01 ± 0.04	599 ± 3.33	10.47 ± 0.14	0.64 ± 0.00	23.99	1.49	18.55
4b + 1 mM CDCA	3.95 ± 0.02	593 ± 2.44	10.49 ± 0.03	0.63 ± 0.01	24.08	1.49	17.98
4b + 2 mM CDCA	3.87 ± 0.02	596 ± 0.96	10.37 ± 0.04	0.63 ± 0.00	24.21	1.49	17.98
4c	2.01 ± 0.00	616 ± 2.94	5.67 ± 0.05	0.57 ± 0.00	46.35	0.24	31.74
7a	1.70 ± 0.01	595 ± 1.92	4.54 ± 0.02	0.63 ± 0.00	48.04	1.49	17.56
7b	2.96 ± 0.02	611 ± 1.77	7.70 ± 0.07	0.63 ± 0.00	31.24	2.26	20.51
7b + 1 mM CDCA	3.30 ± 0.03	619 ± 5.13	8.26 ± 0.11	0.65 ± 0.00	28.61	3.40	23.07
7b + 2 mM CDCA	3.00 ± 0.05	618 ± 0.85	7.79 ± 0.10	0.62 ± 0.01	30.30	3.40	23.07

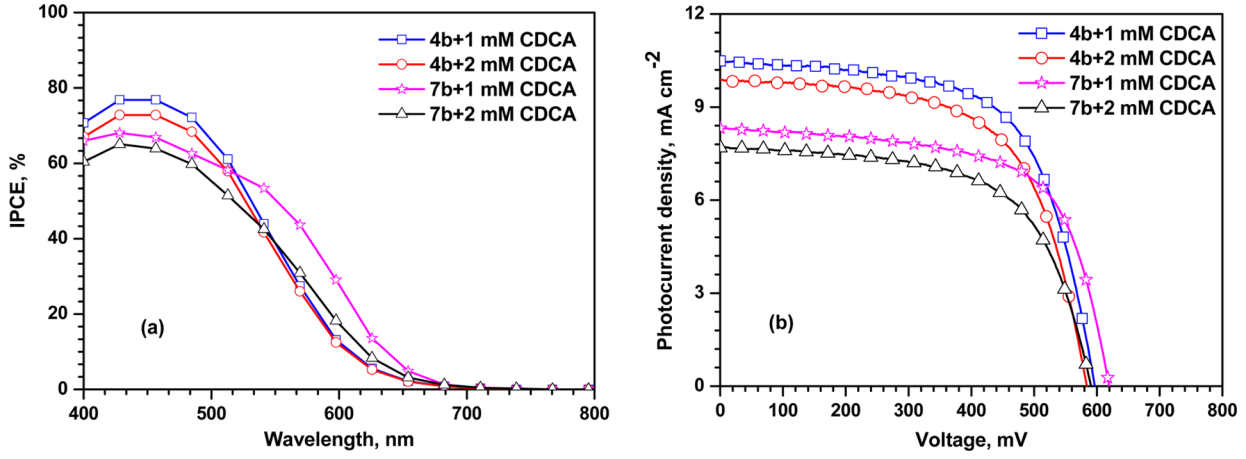

Figure 11. (a) IPCE and (b) *I*–*V* characteristics of DSSCs fabricated using **4b** and **7b** coadsorbed with CDCA.

dyes, the highest occupied molecular orbital (HOMO) is mainly contributed by the phenothiazine unit and the lowest unoccupied molecular orbitals (LUMO) is located over the cyanoacrylic acid acceptor unit and spread up to the phenyl/oligothiophene linkers. In the case of rod-like dyes, the HOMO is also slightly extended into the fluorene unit. Due to the delocalization of HOMO in the fluorene, the HOMO to LUMO electronic transition for the rod-like dyes are expected to occur at the longer wavelength region with appreciable molar extinction coefficients. In general, the HOMO and LUMO are well separated in the T-shaped dyes while a partial overlap between them is present in the rod-like dyes. On the basis of this, a pronounced charge migration from donor to acceptor is predicted on electronic excitation from the HOMO to LUMO for the T-shaped dyes, but the propensity for the charge recombination is high for the rod-like dyes.

Photovoltaic Performance of the Dyes. Finally, DSSCs were fabricated using the organic dyes as sensitizers in TiO_2 photoanodes comprising an ∼12 μm thick transparent layer of 20 nm-sized TiO_2 nanoparticles and ∼4 μm thick scattering layer of 300 nm-sized TiO_2 particles. The performance of the dyes as sensitizers in DSSCs was evaluated by measuring incident photon-to-current conversion efficiency (IPCE) and *I*–*V* characteristics (Figure 10a,b). The photovoltaic responses of the dyes at different wavelengths are consistent with their absorption propensity. In general, the T-shaped dyes (**4a** and **4b**) exhibited high IPCE values (>80%) when compared to that of the rod-like dyes (**7a** and **7b**). The small photocurrent density observed for the dye **4c** is reminiscent of its poor

DOI: 10.1021/am506149q
ACS Appl. Mater. Interfaces 2015, 7, 2249–2262

spectral response resulting from the weak donor−acceptor interactions due to the tilted phenyl linkage.[55] The IPCE spectra for the dyes containing bithiophene linkage (**4b** and **7b**) are broader than that of the thiophene-bridged dyes (**4a** and **7a**). Despite the comparable absorption properties, the low IPCE values observed for the rod-shaped dyes (**7a** and **7b**) are probably a result of dye aggregation on the TiO_2 surface. It is well established that the dye aggregation enhances the excited-state quenching pathways and reduces the electron injection efficiency.[56]

Figure 10b shows the $I-V$ curve of the cells based on as synthesized dyes, and the results are summarized in Table 2. Under the standard global AM1.5 solar conditions, the DSSCs based on dyes follow the order **4b** > **4a** > **7b** > **4c** > **7a** for short circuit current density (J_{SC}) and **4a** > **4c** > **7b** > **4b** ∼ **7a** for open circuit voltage (V_{OC}). Although the rod-shaped dyes show broader and intense absorption in the visible region than the T-shaped dyes, the J_{SC} and V_{OC} with the rod-like dyes are lower than that of the T-shaped dyes. One of the reasons for the poor performance of the rod-like dyes can be attributed to the poor electron collection efficiency from the excited dyes to the conduction band of TiO_2 (*vide infra*).[57] An alternative explanation for the mediocre performance for rod-like organic dyes is their tendency for aggregation that accelerates the quenching of the excited state and adversely affects the performances of DSSCs. Further, the low efficiency for the device based on the dye **4b** when compared to **4a** can be attributed to the higher HOMO level (Figure 8) of the former dye which retards the regeneration of the oxidized dye and higher recombination of photoinjected electrons resulting in overall low V_{OC}.[58]

To gain insight into the aggregation tendency of rod-shaped and T-shaped dyes and their effect on photovoltaic performance, photoanodes comprising dyes **4b** and **7b** and coadsorbed with different concentrations of chenodeoxycholic acid (CDCA) (Figure 11a,b) were constructed. Herein, we preferred the dyes **4b** and **7b** for this study because the organic dyes with an elongated linker are liable to experience significant dye aggregation through strong intermolecular $\pi-\pi$ interactions.[6] As illustrated in Figure 11b, the dye **7b** shows reasonable improvement in J_{SC} and V_{OC} with an addition of 1 mM CDCA as coadsorbent. This can be explained by considering that CDCA with sterically demanding structure can inhibit unfavorable dye aggregation and facilitate electron injection. On the other hand, for the dye **4b**, CDCA addition does not improve the device performance which probably indicates that replacement of dye with CDCA on the TiO_2 surface does not contribute to the inhibition of unwanted processes. While in the case of the dye **7b**, low dye coverage is counterbalanced by reduction of $\pi-\pi$ stacking interactions and thus leads to improvement in photovoltaic performance.[59] Thus, the CDCA addition in this study helps to prove the higher aggregation tendency of rod-shaped dyes than that of T-shaped dyes. Further, we found that on the addition of larger concentrations of CDCA (2 mM) a drop in the efficiency is observed for both the dyes. This can be attributed to two main reasons: (i) A large amount of CDCA may leave protons on the TiO_2 and decrease the conduction band edge, resulting in a loss in V_{OC}.[60] (ii) Since the introduction of CDCA always occupies TiO_2 sites, it decreases the dye coverage which potentially limits further improvement in the photovoltaic performance.[61]

To elucidate the effect of the nature of donor substitution and the π-linker on the performance of DSSCs, electrochemical impedance spectroscopy (EIS) measurements were conducted. Figure 12a shows Nyquist plots for DSSCs that were

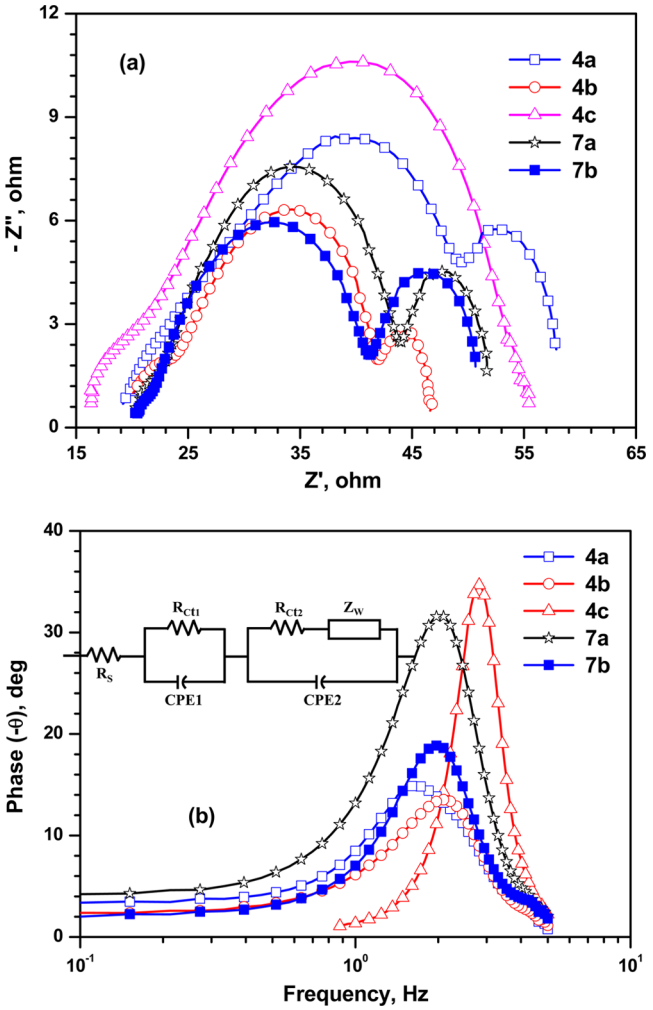

Figure 12. (a) Nyquist plots measured under dark condition and (b) Bode phase plots measured under illumination of the DSSCs fabricated using dyes.

constructed from the measurements under dark condition with a forward bias of −0.70 V. Two semicircles are visible in each Nyquist plot. The smaller semicircles are attributed to the charge transfer at the counter electrode/electrolyte interface and the larger semicircles correspond to the TiO_2/dye/electrolyte interface. There is a substantial difference in the diameter of the large semicircles for each dye, which indicates that charge transfer behavior between TiO_2 and dye or between dye and electrolyte is significantly altered due to attachment position of donor unit and the presence of different linker unit in the dyes. The electron recombination resistance (R_{rec}) obtained from the plots follows the order **4c** > **4a** > **7b** > **4b** > **7a**. This order is fairly similar to the trend observed in V_{OC} (**4a** > **4c** > **7b** > **4b** ∼ **7a**) and indicates that T-shaped configuration of the dyes is beneficial to block the approach of I_3^- ion to TiO_2. The effect of variation in π-spacers is highlighted in view of changes in R_{rec}. It is apparent that the R_{rec} of the dye **4c** is higher than those of the remaining dyes. This may be caused by the introduction of benzene ring which shows a larger dihedral angle between the fluorene and benzene ring and reduces the electron recombination; this leads to improvement in V_{OC}. The

DOI: 10.1021/am506149q
ACS Appl. Mater. Interfaces 2015, 7, 2249−2262

charge transfer resistance (R_{ct2}) obtained from the Nyquist plot under illumination (Figure S6, Supporting Information) assumes the order **7a** > **4c** > **7b** > **4a** > **4b**. This order is largely in agreement with the observed J_{SC} values. It is believed that the lower value of electron transfer resistance will support the electron collection and consequently will play an important role in increasing the cell efficiency. The electron lifetime can be extracted from the angular frequency (ω_{min}) at the midfrequency peak in the Bode phase plot (Figure 12b) by using $\tau_e = 1/\omega_{min}$.[62] The obtained τ_e for both sets of dyes is consistent with their V_{OC} values (see above). The increase in the electron lifetimes for the device that are based on dye **4a** suggests a more effective suppression of the back reaction of injected electrons with I_3^- ions in the electrolyte, which leads to an improvement in V_{OC} values, as well as to a substantial enhancement in the IPCE of the DSSCs. The electron lifetime obtained from the curve fitting of **7b** (Figure S8, Supporting Information) increases after CDCA addition until saturation, while it does not change for the dye **4b**. This indicates that CDCA addition suppresses the aggregation present in rod-shaped dyes and yields an improvement in the photocurrent.

CONCLUSIONS

We have synthesized two types of D-π-A sensitizers featuring phenothiazine donor functionalized via nitrogen (N10) or carbon (C3) and cyanoacrylic acid acceptor/anchoring group yielding either T-shaped or rod-like organic dyes. The conjugation pathway between the donor and acceptor was composed of fluorene and a variable number of thiophene units. The structure of the dye **4c** was confirmed by single crystal XRD and suggests a slip-stacks columnar packing of the molecules in the solid state. Optical measurements indicate that rod-like dyes show broader and red-shifted absorption profiles compared to the T-shaped dyes due to longer conjugation channels in the former. It has been found that the presence of the phenyl unit in the conjugation pathway was manifested in the optical and electrochemical properties by reducing the donor–acceptor interactions, whereas thiophene or bithiophene served as efficient linker and resulted in red-shifted absorption spectra and low-lying LUMO level for the dyes. Though the rod-like dyes exhibited longer wavelength absorption, the T-shaped dyes served as efficient sensitizers in DSSCs and resulted in high efficiency due to the promising V_{OC} and J_{SC} values. The supremacy of T-shaped dyes arises due to higher recombination resistance, lower charge transport resistance, better electron lifetime, and favorable electron injection. Our finding supports that the use of *N*-functionalized phenothiazine with fluorene-based conjugating linker in the dye architecture (T-shaped) is an effective strategy for blocking the electron recombination and to enhance the conversion efficiency.

ASSOCIATED CONTENT

Supporting Information

Copies of ^{1}H and ^{13}C NMR spectra, absorption spectra of the dyes recorded in different solvents, absorption data in different solvents, Cartesian coordinates for the optimized structures, and TDDFT calculation results. This material is available free of charge via the Internet at http://pubs.acs.org.

AUTHOR INFORMATION

Corresponding Author

*E-mail: krjt8fcy@iitr.ernet.in. Phone: +91-1332-285376.

Notes

The authors declare no competing financial interest.

ACKNOWLEDGMENTS

K.R.J.T. thanks the Department of Science and Technology (DST/TSG/PT/2013/09), New Delhi, India, for financial support and for the mass spectral facility under the FIST program. A.B. acknowledges a Senior Research Fellowship from CSIR, New Delhi. The staff at the X-ray diffractometer facility at the Department of Chemistry, Indian Institute of Technology Madras, Chennai, is gratefully acknowledged for the assistance in the structure determination of **4c**.

REFERENCES

(1) O'Regan, B.; Grätzel, M. A Low-Cost, High-Efficiency Solar Cell Based on Dye-Sensitized Colloidal TiO_2 Films. *Nature* **1991**, *353*, 737–740.

(2) Hagfeldt, A.; Boschloo, G.; Sun, L.; Kloo, L.; Pettersson, H. Dye-Sensitized Solar Cells. *Chem. Rev.* **2010**, *110*, 6595–6663.

(3) Nazeeruddin, M. K.; Péchy, P.; Renouard, T.; Zakeeruddin, S. M.; Humphry-Baker, R.; Comte, P.; Liska, P.; Cevey, L.; Costa, E.; Shklover, V.; Spiccia, L.; Deacon, G. B.; Bignozzi, C. A.; Grätzel, M. Engineering of Efficient Panchromatic Sensitizers for Nanocrystalline TiO_2-Based Solar Cells. *J. Am. Chem. Soc.* **2001**, *123*, 1613–1624.

(4) Yella, A.; Lee, H.-W.; Tsao, H. N.; Yi, C.; Chandiran, A. K.; Nazeeruddin, M. K.; Diau, E. W.-G.; Yeh, C.-Y.; Zakeeruddin, S. M.; Grätzel, M. Porphyrin-Sensitized Solar Cells with Cobalt (II/III)–Based Redox Electrolyte Exceed 12% Efficiency. *Science* **2011**, *334*, 629–634.

(5) Burschka, J.; Pellet, N.; Moon, S.-J.; Humphry-Baker, R.; Gao, P.; Nazeeruddin, M. K.; Grätzel, M. Sequential Deposition as a Route to High-Performance Perovskite-Sensitized Solar Cells. *Nature* **2013**, *499*, 316–319.

(6) Liang, M.; Chen, J. Arylamine Organic Dyes for Dye-Sensitized Solar Cells. *Chem. Soc. Rev.* **2013**, *42*, 3453–3488.

(7) Ooyama, Y.; Harima, Y. Photophysical and Electrochemical Properties, and Molecular Structures of Organic Dyes for Dye-Sensitized Solar Cells. *ChemPhysChem* **2012**, *13*, 4032–4080.

(8) Mishra, A.; Fischer, M. K. R.; Bäuerle, P. Metal-Free Organic Dyes for Dye-Sensitized Solar Cells: From Structure: Property Relationships to Design Rules. *Angew. Chem., Int. Ed.* **2009**, *48*, 2474–2499.

(9) Wangdong, Z.; Yiming, C.; Yu, B.; Yinghui, W.; Yushuai, S.; Min, Z.; Fangfang, W.; Chunyue, P.; Peng, W. Efficient Dye-Sensitized Solar Cells with an Organic Photosensitizer Featuring Orderly Conjugated Ethylenedioxythiophene and Dithienosilole Blocks. *Chem. Mater.* **2010**, *22*, 1915–1925.

(10) Lin, R. Y.-Y.; Lin, H.-W.; Yen, Y.-S.; Chang, C.-H.; Chou, H.-H.; Chen, P.-W.; Hsu, C.-Y.; Chen, Y.-C.; Lin, J. T.; Ho, K.-C. 2,6-Conjugated Anthracene Sensitizers for High-Performance Dye-Sensitized Solar Cells. *Energy Environ. Sci.* **2013**, *6*, 2477–2486.

(11) Yu, C.-C.; Jiang, K.-J.; Huang, J.-H.; Zhang, F.; Bao, X.; Wang, F.-W.; Yang, L.-M.; Song, Y. Novel Pyrene-Based Donor-Acceptor Organic Dyes for Solar Cell Application. *Org. Electron.* **2013**, *14*, 445–450.

(12) Yang, F.; Akhtaruzzaman, M.; Islam, A.; Jin, T.; El-Shafei, A.; Qin, C.; Han, L.; Alamry, K. A.; Kosa, S. A.; Hussein, M. A.; Asiri, A. M.; Yamamoto, Y. Structure–Property Relationship of Naphthalene Based Donor–π–Acceptor Organic Dyes for Dye-Sensitized Solar Cells: Remarkable Improvement of Open-Circuit Photovoltage. *J. Mater. Chem.* **2012**, *22*, 22550–22557.

(13) Wang, Z.-S.; Koumura, N.; Cui, Y.; Takahashi, M.; Sekiguchi, H.; Mori, A.; Kubo, T.; Furube, A.; Hara, K. Hexylthiophene-Functionalized Carbazole Dyes for Efficient Molecular Photovoltaics: Tuning of Solar-Cell Performance by Structural Modification. *Chem. Mater.* **2008**, *20*, 3993–4003.

DOI: 10.1021/am506149q
ACS Appl. Mater. Interfaces 2015, 7, 2249–2262

(14) Haid, S.; Marszalek, M.; Mishra, A.; Wielopolski, M.; Teuscher, J.; Moser, J.-E.; Humphry-Baker, R.; Zakeeruddin, S. M.; Grätzel, M.; Bäuerle, P. Significant Improvement of Dye-Sensitized Solar Cell Performance by Small Structural Modification in π-Conjugated Donor−Acceptor Dyes. *Adv. Funct. Mater.* **2012**, *22*, 1291−1302.
(15) Kim, G. W.; Cho, M. J.; Yu, Y. J.; Kim, Z. H.; Jin, J. I.; Kim, D. Y.; Choi, D. H. Red Emitting Phenothiazine Dendrimers Encapsulated 2-{2-[2-(4-Dimethylaminophenyl)vinyl]-6-methylpyran-4-ylidene}-malononitrile Derivatives. *Chem. Mater.* **2007**, *19*, 42−50.
(16) Achar, B. N.; Ashok, M. A. Electrical Measurements and Thermal Kinetics Study of Phenothiazine and a Few of Its Derivatives. *Mater. Chem. Phys.* **2008**, *108*, 8−15.
(17) Hauck, M.; Schonhaber, J.; Zucchero, A. J.; Hardcastle, K. I.; Müller, T. J. J.; Bunz, U. H. F. Phenothiazine Cruciforms: Synthesis and Metallochromic Properties. *J. Org. Chem.* **2007**, *72*, 6714−6725.
(18) Tian, H.; Yang, X.; Chen, R.; Pan, Y.; Li, L.; Hagfeldt, A.; Sun, L. Phenothiazine Derivatives for Efficient Organic Dye-Sensitized Solar Cells. *Chem. Commun.* **2007**, 3741−3743.
(19) Kim, S. H.; Kim, H. W.; Sakong, C.; Namgoong, J. W.; Park, S. W.; Ko, M. J.; Lee, C. H.; Lee, W. I.; Kim, J. P. Effect of Five-Membered Heteroaromatic Linkers to the Performance of Phenothiazine-Based Dye-Sensitized Solar Cells. *Org. Lett.* **2011**, *13*, 5784−5787.
(20) Yang, C. J.; Chang, Y. J.; Watanabe, M.; Hon, Y. S.; Chow, T. J. Phenothiazine Derivatives as Organic Sensitizers for Highly Efficient Dye-Sensitized Solar Cells. *J. Mater. Chem.* **2012**, *22*, 4040−4049.
(21) Hart, A. S.; Bikram, K. C. C.; Subbaiyan, N. K.; Paul, A. K.; D'Souza, F. Phenothiazine-Sensitized Organic Solar Cells: Effect of Dye Anchor Group Positioning on the Cell Performance. *ACS Appl. Mater. Interfaces* **2012**, *4*, 5813−5820.
(22) Hua, Y.; Chang, S.; Wang, H.; Huang, D.; Zhao, J.; Chen, T.; Wong, W.-Y.; Wong, W.-K.; Zhu, X. New Phenothiazine-Based Dyes for Efficient Dye-Sensitized Solar Cells: Positioning Effect of a Donor Group on the Cell Performance. *J. Power Sources* **2013**, *243*, 253−259.
(23) Hua, Y.; Chang, S.; Huang, D.; Zhou, X.; Zhu, X.; Zhao, J.; Chen, T.; Wong, W.-Y.; Wong, W.-K. Significant Improvement of Dye-Sensitized Solar Cell Performance Using Simple Phenothiazine-Based Dyes. *Chem. Mater.* **2013**, *25*, 2146−2153.
(24) Hua, Y.; Chang, S.; He, J.; Zhang, C.; Zhao, J.; Chen, T.; Wong, W.-Y.; Wong, W.-K.; Zhu, X. Molecular Engineering of Simple Phenothiazine-Based Dyes To Modulate Dye Aggregation, Charge Recombination, and Dye Regeneration in Highly Efficient Dye-Sensitized Solar Cells. *Chem.—Eur. J.* **2014**, *20*, 6300−6308.
(25) Ni, J.-S.; You, J.-H.; Hung, W.-I; Kao, W.-S.; Chou, H.-H.; Lin, J. T. Organic Dyes Incorporating the Dithieno[3′,2′:3,4;2″,3″:5,6]-benzo[1,2-*c*]furazan Moiety for Dye Sensitized Solar Cells. *ACS Appl. Mater. Interfaces* **2014**, *6*, 22612−22621.
(26) Wang, S.; Wang, H.; Guo, J.; Tang, H.; Zhao, J. Influence of the Terminal Electron Donor in D-D-π-A Phenothiazine Dyes for Dye-Sensitized Solar Cells. *Dyes Pigm.* **2014**, *109*, 96−104.
(27) Cheng, M.; Yang, X.; Zhang, F.; Zhao, J.; Sun, L. Tuning the HOMO and LUMO Energy Levels of Organic Dyes with *N*-Carboxomethylpyridinium as Acceptor To Optimize the Efficiency of Dye-Sensitized Solar Cells. *J. Phys. Chem. C* **2013**, *117*, 9076−9083.
(28) Wan, Z.; Jia, C.; Duan, Y.; Zhou, L.; Lin, Y.; Shia, Y. Phenothiazine−Triphenylamine Based Organic Dyes Containing Various Conjugated Linkers for Efficient Dye-Sensitized Solar Cells. *J. Mater. Chem.* **2012**, *22*, 25140−25147.
(29) Baheti, A.; Gajjela, S. R.; Balaya, P.; Thomas, K. R. J. Synthesis, Optical, Eectrochemical and Photovoltaic Properties of Organic Dyes Containing Trifluorenylamine Donors. *Dyes Pigm.* **2015**, *113*, 78−86.
(30) Baheti, A.; Thomas, K. R. J.; Lee, C.-P.; Li, C.-T.; Ho, K.-C. Organic Dyes Containing Fluoren-9-ylidene Chromophores for Efficient Dye-Sensitized Solar Cells. *J. Mater. Chem. A* **2014**, *2*, 5766−5779.
(31) Baheti, A.; Thomas, K. R. J.; Lee, C.-P.; Ho, K.-C. Synthesis and Characterization of Dianchoring Organic Dyes Containing 2,7-Diaminofluorene Donors as Efficient Sensitizers for Dye-Sensitized Solar Cells. *Org. Electron.* **2013**, *14*, 3267−3276.
(32) Thomas, K. R. J.; Baheti, A. Fluorene Based Organic Dyes for Dye Sensitised Solar Cells: Structure-Property Relationships. *Mater. Technol.* **2013**, *28*, 71−87.
(33) Baheti, A.; Thomas, K. R. J.; Lee, C.-P.; Ho, K.-C. Fine Tuning the Performance of DSSCs by Variation of the π-Spacers in Organic Dyes that Contain a 2,7-Diaminofluorene Donor. *Chem. Asain J.* **2012**, *7*, 2942−2954.
(34) Baheti, A.; Singh, P.; Lee, C.-P.; Thomas, K. R. J.; Ho, K.-C. 2,7-Diaminofluorene-Based Organic Dyes for Dye-Sensitized Solar Cells: Effect of Auxiliary Donor on Optical and Electrochemical Properties. *J. Org. Chem.* **2011**, *76*, 4910−4920.
(35) Frisch, M. J.; Trucks, G. W.; Schlegel, H. B.; Scuseria, G. E.; Robb, M. A.; Cheeseman, J. R.; Scalmani, G.; Barone, V.; Mennucci, B.; Petersson, G. A.; Nakatsuji, H.; Caricato, M.; Li, X.; Hratchian, H. P.; Izmaylov, A. F.; Bloino, J.; Zheng, G.; Sonnenberg, J. L.; Hada, M.; Ehara, M.; Toyota, K.; Fukuda, R.; Hasegawa, J.; Ishida, M.; Nakajima, T.; Honda, Y.; Kitao, O.; Nakai, H.; Vreven, T.; Montgomery, J. A.; Peralta, J. E.; Ogliaro, F.; Bearpark, M.; Heyd, J. J.; Brothers, E.; Kudin, K. N.; Staroverov, V. N.; Kobayashi, R.; Normand, J.; Raghavachari, K.; Rendell, A.; Burant, J. C.; Iyengar, S. S.; Tomasi, J.; Cossi, M.; Rega, N.; Millam, N. J.; Klene, M.; Knox, J. E.; Cross, J. B.; Bakken, V.; Adamo, C.; Jaramillo, J.; Gomperts, R.; Stratmann, R. E.; Yazyev, O.; Austin, A. J.; Cammi, R.; Pomelli, C.; Ochterski, J. W.; Martin, R. L.; Morokuma, K.; Zakrzewski, V. G.; Voth, G. A.; Salvador, P.; Dannenberg, J. J.; Dapprich, S.; Daniels, A. D.; Farkas, O.; Foresman, J. B.; Ortiz, J. V.; Cioslowski, J.; Fox, D. J. *Gaussian 09*, Revision A.02; Gaussian, Inc.: Wallingford, CT, 2009.
(36) Becke, A. D. A New Mixing of Hartree−Fock and Local Density-Functional Theories. *J. Chem. Phys.* **1993**, *98*, 1372−1377.
(37) Lee, C.; Yang, W.; Parr, R. G. Development of the Colle-Salvetti Correlation-Energy Formula into a Functional of the Electron Density. *Phys. Rev. B* **1988**, *37*, 785−789.
(38) Sheldrick, G. M. *SHELXS-97: Program for Crystal Structure Determination*; University of Göttingen: Germany, 1997.
(39) Sheldrick, G. M. *SHELXL-97: Program for the Refinement of Crystal Structure*; University of Göttingen: Germany, 1997.
(40) Farrugia, L. J. WinGX and ORTEP for Windows: An Update. *J. Appl. Crystallogr.* **2012**, *45*, 849−854.
(41) Hartwig, J. F. Transition Metal Catalyzed Synthesis of Arylamines and Aryl Ethers from Aryl Halides and Triflates: Scope and Mechanism. *Angew. Chem., Int. Ed.* **1998**, *37*, 2046−2067.
(42) Miyaura, N.; Suzuki, A. Palladium-Catalyzed Cross-Coupling Reactions of Organoboron Compounds. *Chem. Rev.* **1995**, *95*, 2457−2483.
(43) Stille, J. K. The Palladium-Catalyzed Cross-Coupling Reactions of Organotin Reagents with Organic Electrophiles [New Synthetic Methods (58)]. *Angew. Chem., Int. Ed.* **1986**, *25*, 508−523.
(44) Curtis, M. D.; Cao, J.; Kampf, J. W. Solid-State Packing of Conjugated Oligomers: From π-Stacks to the Herringbone Structure. *J. Am. Chem. Soc.* **2004**, *126*, 4318−4328.
(45) Pei, K.; Wu, Y.; Islam, A.; Zhang, Q.; Han, L.; Tian, H.; Zhu, W. Constructing High-Efficiency D−A−π−A-Featured Solar Cell Sensitizers: A Promising Building Block of 2,3-Diphenylquinoxaline for Antiaggregation and Photostability. *ACS Appl. Mater. Interfaces* **2013**, *5*, 4986−4995.
(46) Cornil, J.; Beljonne, D.; Calbert, J.-P.; Brédas, J.-L. Interchain Interactions in Organic π-Conjugated Materials: Impact on Electronic Structure, Optical Response, and Charge Transport. *Adv. Mater.* **2001**, *13*, 1053−1067.
(47) Li, R.; Lv, X.; Shi, D.; Zhou, D.; Cheng, Y.; Zhang, G.; Wang, P. Dye-Sensitized Solar Cells Based on Organic Sensitizers with Different Conjugated Linkers: Furan, Bifuran, Thiophene, Bithiophene, Selenophene, and Biselenophene. *J. Phys. Chem. C* **2009**, *113*, 7469−7479.
(48) Chen, B.-S.; Chen, D.-Y.; Chen, C.-L.; Hsu, C.-W.; Hsu, H.-C.; Wu, K.-L.; Liu, S.-H.; Chou, P.-T.; Chi, Y. Donor-Acceptor Dyes with Fluorine Substituted Phenylene Spacer for Dye-Sensitized Solar Cells. *J. Mater. Chem.* **2011**, *21*, 1937−1945.

DOI: 10.1021/am506149q
ACS Appl. Mater. Interfaces 2015, 7, 2249−2262

(49) Teng, C.; Yang, X.; Yang, C.; Li, S.; Cheng, M.; Hagfeldt, A.; Sun, L. Molecular Design of Anthracene-Bridged Metal-Free Organic Dyes for Efficient Dye-Sensitized Solar Cells. *J. Phys. Chem. C* **2010**, *114*, 9101−9110.
(50) Nazeeruddin, M. K.; Zakeeruddin, S. M.; Humphry-Baker, R.; Jirousek, M.; Liska, P.; Vlachopoulos, N.; Shklover, V.; Fischer, C.-H.; Grätzel, M. Acid−Base Equilibria of (2,2′-Bipyridyl-4,4′-dicarboxylic acid)ruthenium(II) Complexes and the Effect of Protonation on Charge-Transfer Sensitization of Nanocrystalline Titania. *Inorg. Chem.* **1999**, *38*, 6298−6305.
(51) Baheti, A.; Tyagi, P.; Thomas, K. R. J.; Hsu, Y.-C.; Lin, J. T. Simple Triarylamine-Based Dyes Containing Fluorene and Biphenyl Linkers for Efficient Dye-Sensitized Solar Cells. *J. Phys. Chem. C* **2009**, *113*, 8541−8547.
(52) Green, A. N. M.; Palomares, E.; Haque, S. A.; Kroon, J. M.; Durrant, J. R. Charge Transport versus Recombination in Dye-Sensitized Solar Cells Employing Nanocrystalline TiO_2 and SnO_2 Films. *J. Phys. Chem. B* **2005**, *109*, 12525−1533.
(53) Grätzel, M. Photoelectrochemical Cells. *Nature* **2001**, *414*, 338−344.
(54) Parr, R. G.; Yang, W. T. Density-Functional Theory of the Electronic Structure of Molecules. *Annu. Rev. Phys. Chem.* **1995**, *46*, 701−728.
(55) Chang, Y. J.; Chow, T. J. Triaryl Linked Donor Acceptor Dyads for High-Performance Dye-Sensitized Solar Cells. *Tetrahedron* **2009**, *65*, 9626−9632.
(56) Listorti, A.; O'Regan, B.; Durrant, J. R. Electron Transfer Dynamics in Dye-Sensitized Solar Cells. *Chem. Mater.* **2011**, *23*, 3381−3399.
(57) Seo, K. D.; You, B. S.; Choi, I. T.; Ju, M. J.; You, M.; Kang, H. S.; Kim, H. K. Dual-Channel Anchorable Organic Dyes with Well-Defined Structures for Highly Efficient Dye-Sensitized Solar Cells. *J. Mater. Chem. A* **2013**, *1*, 9947−9953.
(58) Wielopolski, M.; Kim, J.-H.; Jung, Y.-S.; Yu, Y.-J.; Kay, K.-Y.; Holcombe, T. W.; Zakeeruddin, S. M.; Grätzel, M.; Moser, J.-E. Position-Dependent Extension of π-Conjugation in D-π-A Dye Sensitizers and the Impact on the Charge-Transfer Properties. *J. Phys. Chem. C* **2013**, *117*, 13805−13815.
(59) Capodilupo, A. L.; Marco, L. D.; Fabiano, E.; Giannuzzi, R.; Scrascia, A.; Clarlucci, C.; Corrente, G. A.; Cipolla, M. P.; Gigli, G.; Ciccarella, G. New Organic Dyes Based on a Dibenzofulvene Bridge for Highly Efficient Dye-Sensitized Solar Cells. *J. Mater. Chem. A* **2014**, *2*, 14181−14188.
(60) Qu, S. Y.; Wu, W. J.; Hua, J. L.; Kong, C.; Long, Y. T.; Tian, H. New Diketopyrrolopyrrole (DPP) Dyes for Efficient Dye-Sensitized Solar Cells. *J. Phys. Chem. C* **2010**, *114*, 1343−1349.
(61) Ooyama, Y.; Harima, Y. Molecular Designs and Syntheses of Organic Dyes for Dye-Sensitized Solar Cells. *Eur. J. Org. Chem.* **2009**, 2903−2934.
(62) van de Lagemaat, J.; Park, N.-G.; Frank, A. J. Influence of Electrical Potential Distribution, Charge Transport, and Recombination on the Photopotential and Photocurrent Conversion Efficiency of Dye-Sensitized Nanocrystalline TiO_2 Solar Cells: A Study by Electrical Impedance and Optical Modulation Techniques. *J. Phys. Chem. B* **2000**, *104*, 2044−2052.

DOI: 10.1021/am506149q
ACS Appl. Mater. Interfaces 2015, 7, 2249−2262